ENHANCEMENT OF JET SHEAR LAYER MIXING AND SURFACE HEAT TRANSFER BY MEANS OF ACOUSTIC DISTURBANCES

A Thesis Submitted to
the Graduate School of Engineering and Sciences of
İzmir Institute of Technology
in Partial Fulfillment of the Requirements for the Degree of

MASTER OF SCIENCE

in Mechanical Engineering

by
Orçun KOR

December 2010
İZMİR

We approve the thesis of **Orçun KOR**

Assist. Prof. Dr. Ünver ÖZKOL
Supervisor

Assoc. Prof. Dr. Moghtada MOBEDİ
Committee Member

Assoc. Prof. Dr. Serhan KÜÇÜKA
Committee Member

17 December 2010

Prof. Dr. Metin TANOĞLU
Head of the Department of
Mechanical Engineering

Prof. Dr. Durmuş Ali DEMİR
Dean of the Graduate School of
Engineering and Sciences

ACKNOWLEDGMENTS

I would like to express my sincere gratitude to my supervisor Assist. Prof. Dr. Ünver ÖZKOL for his valuable advises and guidance through the thesis.

All of my lab-mates, but especially Ali AKÇA and Shankaransh SRIVASTAVA played great role in my experimental studies. They were always near me when I need help in my experimental studies, even in the sleepless night shifts. Thanks to them for their precious efforts

Lastly, I would like to thank my dear mother, who has always encouraged and supported me, as she did so during my graduate studies.

ABSTRACT

ENHANCEMENT OF JET SHEAR LAYER MIXING AND SURFACE HEAT TRANSFER BY MEANS OF ACOUSTIC DISTURBANCES

The objective of this thesis is to investigate how the surface heat transfer of an impinging jet flow can be increased by acoustic actuation of which changes the turbulence characteristics of the flow. This work is built upon experimental studies which includes flow visualization experiments and surface heat transfer measurements. A loudspeaker system which is controlled by means of a function generator is used for the purpose of actuating impinging jet flow. Acoustic waves in different waveforms, frequencies and amplitudes which are generated by the loudspeaker reaches the jet nozzle, resulting in the formation of an oscillating component on the mean nozzle velocity since the actuation itself is in the form of a periodic fluctuation. It is this oscillating component that actuates the shear layer of the jet flow. Reynolds number is kept at 10.000 for all experimental cases. Influence of nozzle geometry is investigated by using sudden and smooth contracting (with a curvature of 5 degree polynomial) nozzles. Dimensionless nozzle-to-plate spacing is adjusted between 2, 4 and 6. Strouhal number, which is the non-dimensional form of actuation frequency is changed between $0 < St < 1$. The amplifier, which is used for generating sine and square waves, is set for 1.5 and 2 Volts amplitudes.

ÖZET

JET SINIR TABAKASINDAKI KARIŞIMIN VE YÜZEY ISI TRANSFERININ AKUSTIK TITREŞIMLER ILE ARTTIRILMASI

Bu çalışmada, yüzeye çarpan bir jet akışının yüzey ısı transferi karakteristiklerinin, akışın türbülans özelliklerini etkildiği bilinen akustik titreşim uyarılarının uygulanması durumunda nasıl bir değişim gösterdiği araştırılmıştır. Çalışmamız, akış görüntüleme ve ısı transferi ölçümlerini kapsayan deney verilerine dayanmaktadır. Akustik titreşimler, bir fonksiyon üreteci ve amplifikatör yardımıyla kontrol edilen bir hoparlör vasıtasıyla elde edilmiştir. Farklı dalga formlarına, frekanslara ve genliklere sahip akustik dalgalar yardımıyla jet çıkış bölgesinde küçük dalgalanmalar yaratılmış, böylece jet akışı sınır tabakası uyarılmıştır. Reynolds sayısı tüm deneylerde 10.000 mertebesinde tutulmuştur. Jet geometrisinin etkisinin incelenmesi amacıyla, ani ve yumuşak (yüzeyi beşinci dereceden bir paraboldan oluşan) daralan lülelerin etkisi gözlenmiştir. Boyutsuz lüle-çarpma yüzeyi mesafesi farklı deneylerde 2, 4 ve 6 olarak ayarlanmıştır. Akustik uyarı frekansının boyutsuz ifadesi olan Strouhal sayısı 0 ile 1 aralığında alınmıştır. Akustik dalga formu olarak sinüs ve kare formları kullanılmış, dalga genliğinin 1.5 ve 2 Volt olması durumları karşılaştırılmıştır.

TABLE OF CONTENTS

LIST OF FIGURES

LIST OF TABLES

LIST OF SYMBOLS

A	Area of heater surface	m^2
A_{cr}	Cross sectional area of heater surface	m^2
c_p	Specific heat capacity	J/kgK
CN	Contracting nozzle	
D	Jet diameter	m
f	Actuation frequency	1/s
h	Convective heat transfer coefficient	W/m^2K
I	Turbulence intensity	
k	Conductive heat transfer coefficient	W/mK
L	Length of the heater	m
Nu	Nusselt number	
Pr	Prandtl number	
Q	Heat applied to the test section	W
q''	Heat flux	W/m^2
Re	Reynolds number	
St	Strouhal number	
SD	Sudden contraction	
SM	Smooth contraction	
T	Temperature	°C
u	Axial velocity	m/s
u^1	Fluctuating axial velocity	m/s
$\bar{u}$	Mean axial velocity	m/s
u	Uncertainty	
v	Radial velocity	m/s
v^1	Fluctuating radial velocity	m/s
$\bar{v}$	Mean radial velocity	m/s
x	Radial distance of the jet	m
X	Radial direction coordinate	
z	Axial distance of the jet	m
Z	Axial direction coordinate	
$\dot{\forall}$	Volumetric flow rate	m^3/s

Greek letters

Δ	Difference	
ν	Kinematic viscosity	m^2/s
μ	Dynamic viscosity	kg/ms

Subscript

A	Axial
c	Centerline
j	Jet
max	Maximum
min	Minimum
R	Radial
w	water

CHAPTER 1

INTRODUCTION

Jet impingement is a widely used technique where higher rates of heat or mass transfer are required. A single gas jet impinging normally on a surface may be used to achieve enhanced coefficients for convective heating, cooling or drying. It is widely used in industrial applications such as annealing of metals, cooling of gas turbine blades, cooling in grinding process, tempering of glass plate, drying of textile and paper products. Especially, for electronic components which need highly efficient heat removals, jet impingement cooling offers suitable solutions.

Jet impingement cooling technique uses fluid more effectively. As compared with the forced convection cooling by confined flow parallel on cooled surface, jet impingement offers at about three times higher heat transfer coefficient at a given flow speed due to the thinner boundary layer inherent to the jet impingement, as plotted in Figure 1.1. Often the spent fluid after the impingement serves to further mixing of the surrounding fluid. Zuckerman et al. (2005) reports that given a required heat transfer coefficient, the flow required from an impinging jet may be two orders of magnitude smaller than that required for a cooling using a free wall-parallel flow. The impingement cooling approach offers a compact hardware arrangement with no addition moving parts.

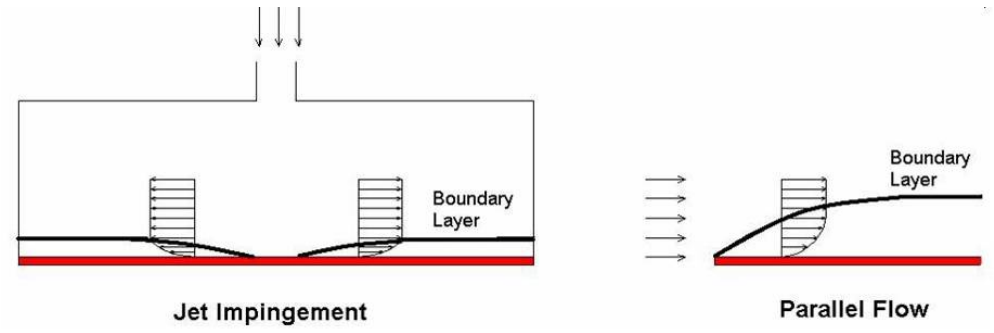

Figure 1.1. Comparison between boundary layer of jet impingement and parallel flow

1.1. Types of Jet Impingement

Impinging jets can be mainly categorized into two groups as gas jets and liquid jets by type of working coolant. A classification offered by Wolf et al. (1993) divides the impinging jet flow into five groups, from a hydrodynamic point of view: free-surface, plunging, submerged, confined and wall jets. In this hydrodynamic classification, the distinguishing feature is the way how the flow interacts with the surface and the ambient fluid, as it is schematized in Figure 1.2. The free-surface jet is injected to an immiscible atmosphere (liquid into gas), and the liquid travels relatively unimpeded into the impingement surface. The plunging jet differs only in that it impinges into a pool of liquid covering the surface, where the depth of the pool is less than the nozzle-to-surface spacing. The submerged jet is injected directly into a miscible atmosphere (liquid into liquid), and the confined jet is injected into a region bounded by the impingement surface and nozzle plate. The wall jet flows parallel to the surface and occurs in both free-surface and submerged configurations.

A combination of confined and a submerged type jet is used for this study. These kinds of jets are usually found to be suitable for a compact and efficient electronic cooling application of which this thesis is stemmed from.

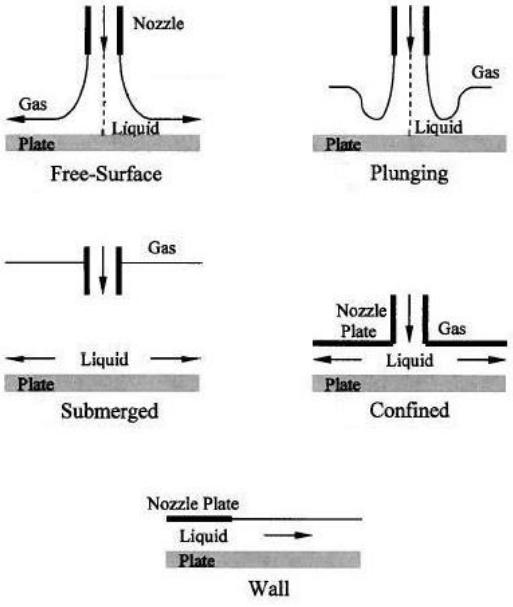

Figure 1.2. Different types of jet impingement
(Source: Wolf et al. 1993)

It's the Reynolds number, what determines and categorizes jet behaviour, where characteristic length scale is the jet nozzle diameter. Zuckerman and Lior (2005) suggested that the flow field exhibits laminar flow properties at Re < 1000, the flow displays turbulent features at Re > 3000 and a transition region occurs between these two regimes.

The jet can also be classified with respect to its shape such as circular, rectangular or slot jets. Another classification addresses the number of jet nozzles: single and multi jets (jet arrays).

Another type of jet is the synthetic jet (Figure 1.3). A synthetic jet flow is created by pulsating jet with zero net mass flux. Normally, a jet requires an external source of fluid, such as piped-in compressed air or pumping and plumbing for water. Synthetic jets have been investigated by researchers, since they do not require plumbing as it is used to in traditional continuous jets. Synthetic jets use ambient fluid, and, when properly designed, can be much more efficient. Synthetic jet flow can be developed in a number of ways, such as with an electromagnetic driver, a piezoelectric driver, or a mechanical driver like a piston. Zhang et al. (2006) defines synthetic jet such that, it is a jet-like mean fluid motion formed by time-periodic, alternate suction and ejection of fluid through an orifice bounding a small cavity, by the time periodic motion of a diaphragm that is built into one of the walls of the cavity. As it can be seen in Figure 1.3, the mechanism moves a membrane or diaphragm up and down hundreds of times per second, sucking the surrounding fluid into a chamber and then expelling it. Although the mechanism is fairly simple, extremely fast cycling requires high-level of engineering to produce a device that will last in an industrial applications.

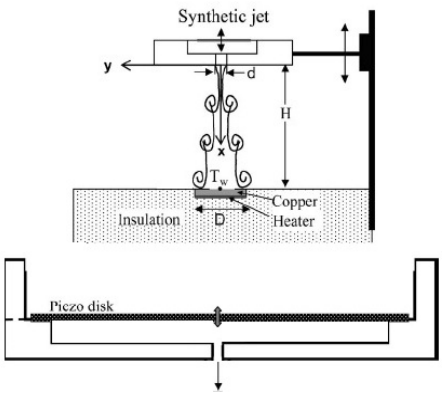

Figure 1.3. Synthetic jet
(Source: Pavlova et al. 2006)

1.2. Hydrodynamics of Jet Impingement

Major factors of the hydrodynamics of jet flow are the initial flow state, the type of the stationary ambient fluid and the location of the impinging plate from the nozzle.

Typically, the jet is turbulent and, at the nozzle exit, is characterized by a uniform velocity profile. In its initial stage of development, the jet is surrounded by a mixing layer, with a core of irrotational flow in the jet center. However, with increasing distance from the exit, momentum exchange between the jet and the ambient causes the free boundary of the jet to broaden and the potential core, within which the uniform exit velocity is retained, to contract. Velocity profile starts to become non-uniform and center velocity decreases as the distance between the fluid and the nozzle exit increases.

In the deflection zone, the jet decelerates in axial direction, and starts to accelerate in radial direction. Fluid velocity continues to increase in radial direction, but since the ambient fluid has zero momentum, it starts to decelerate after a while, and consequently, decays totally.

The impingement jet flow where impinging occurs orthogonally on a plane surface is commonly divided into four zones (Figure 1.4).

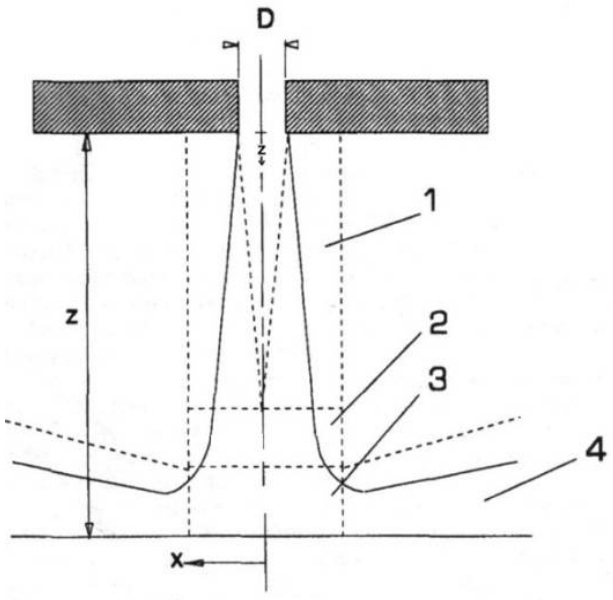

Figure 1.4. Zones in an impinging jet: 1, initial mixing zone; 2,established jet; 3, deflection zone; 4, wall jet (Source: Jambunathan et al. 1992)

A substantial and comprehensive definition, which points out the key points of impinging jet flow step-by-step, has been suggested by Jambunathan et al. (1992) as follows:

(1) There is a developing flow zone where fluid from the surroundings is entrained into the jet, thus reducing the jet velocity. Characteristic of this region is that there is a mixing region where the shear is high surrounding a core region where the fluid velocity (U_c) is almost equal to the nozzle exit velocity (U_{inlet}). The core region is often referred as the potential core. Commonly, end of the core region is defined as the point where $U_c=0.95U_{inlet}$. Gautner et al. (1970) showed that end of the core is at six nozzle diameters.

(2) At greater nozzle to plate spacing the axial velocities reduce with increasing distance from the nozzle exit. Schlichting (1968) showed that the fall of the centerline velocity and the jet half width will be directly proportional to the axial distance from the end of the potential core.

(3) The region near the impingement plate is often referred to as the deflection zone where there is a rapid decrease in axial velocity and a corresponding rise in static pressure. The measurements of Tani and Komatsu (1966) showed that this zone extends approximately two nozzle diameters from the plate surface.

(4) After the flow impinges to the wall, flow turns to radial direction. This region is called the wall-jet region. In this region the radial velocity rises rapidly to a maximum near to the wall and then falls to zero at greater distance from the wall. The wall jet exhibits higher levels of heat transfer than parallel flow. This appears to be due to turbulence generated by the shear between wall jet and the ambient fluid, which is transported to the boundary layer at the heat transfer surface.

1.3. Jet Parameters

The heat transfer characteristic of an impinging jet is depends on many parameters such as Reynolds number (Re), Prandtl number (Pr), dimensionless form of nozzle-to-plate spacing (Z/D) and heated plate length (L/D), and jet exit velocity profile.

In addition to these, the effects of nozzle geometry, flow confinement, turbulence, initial turbulence intensity, recovery factor, dissipation of jet temperature are shown to be significant on heat transfer coefficient.

In an acoustically actuated jet, parameters like actuator's position, actuation amplitude, frequency and waveform which enhance and induce turbulent structures are thought to be significant parameters, as well. It has to be said that the dimensionless number dealing for the effect of actuation frequency on jet impingement is called the Strouhal number (St).

Formulations defining those dimensionless numbers are,

$$Re = \frac{U_{inlet} D}{\nu} \tag{1.1}$$

$$St = \frac{fD}{U_{inlet}} \tag{1.2}$$

$$\frac{Z}{D} \tag{1.3}$$

$$\frac{L}{D} \tag{1.4}$$

$$Pr = \frac{c_p \mu}{k} \tag{1.5}$$

Where, U_{inlet} is jet inlet velocity, D is nozzle diameter, v is fluid's kinematic viscosity, f is the actuation frequency, Z is nozzle-to-plate spacing, L is the length of heated plate, c_p is specific heat capacity and, k is conductive heat transfer coefficient and μ is the dynamic viscosity.

1.4. Motivation

As it will be detailed below, literature survey addresses that heat transfer coefficient in a jet impingement application depends on its turbulence intensity and the radial velocity gradient in the stagnation zone. In turn, both quantities depend on the nozzle geometry and the nozzle to surface spacing (Z) as mentioned in jet parameters and hydrodynamics of jet flow. Objective of many jet applications is to increase heat transfer coefficients on the target hot plate by manipulating one or more of the parameters mentioned.

The objective of this thesis is to investigate how the surface heat transfer of an impinging jet flow can be increased by acoustic actuation of which changes the turbulence characteristics of the flow. The acoustic actuation method is forcing the sound waves to the jet flows, resulting that the flow and heat transfer characteristics are affected by the forcing frequencies. Thus, the heat transfer rates can be enhanced or reduced on the impingement surface by forcing the flow with the proper excitation frequency.

Acoustic (pressure) wave is generated by the loudspeaker. Wave travels along the flow system and reaches the jet nozzle where it generates an oscillating component on the mean nozzle velocity since the actuation itself is in the form of a periodic fluctuation. It is this oscillating component that excites the shear layer of the jet flow. The amplitude, frequency and form of the wave generated by loudspeaker can easily be changed and therefore, its operation is very straightforward.

CHAPTER 2

LITERATURE SURVEY

Over the past few decades, numerous studies have been performed about jet impingement. Objective of this chapter is to summarize the literature written about the subjects that are relevant with the scope of this thesis.

Since there are too many different applications of jet impingement for different purposes, the literature surveyed has been limited and, especially studies concerning about round confined jets and their actuation mechanisms are reviewed.

2.1. Effects of Radial Boundaries and Nozzle-to-Plate Spacing

Radial boundaries, which confines impinging the jet flow from both sides, and nozzle-to-plate spacing which is the axial distance between nozzle exit and cooled plate are the dominant geometric parameters affecting the heat transfer characteristics of jet impingement.

An analytical solution which has been performed by Sibulkin (1952) that is investigating heat transfer at stagnation point in a laminar flow shows that Nusselt number should remain roughly constant in the core region and reduce downstream the core.

Gardon and Akfirat (1965) investigated the axial variations of velocity and turbulence for jet, showing that the turbulence intensity in a free jet could reach 30 percent at approximately the eight nozzle diameters (Z/D=8) downstream of the nozzle. Nozzle-to-plate spacing where the maximum turbulence intensity occurs, appears to coincide with that of the maximum stagnation point heat transfer. Schulunder and Gnielinski's (1967) results also points out a similar suggestion that both the maximum turbulence and the maximum stagnation point heat transfer occurs at Z/D=7.5. Gardon and Akfirat (1965) suggested that the increasing level of turbulence causes the heat transfer rate to increase. The increase in the heat transfer rate ceases when the increase in turbulence does not compensate for the fall in the jet velocity. Part of our aim in this study is in the same line with this finding which is to promote the turbulence in jet shear layer to increase the heat transfer.

The radial variation of heat transfer coefficient measured by Gardon et al. (1962) are given in Figure 2.1. Their results show a local maxima in the heat transfer coefficient for z/D<6. The heat transfer coefficient for an impinging circular jet is seen to increase between the stagnation point and x/D=0.5 for a small jet-to-plate distance (Z/D<6). A second maximum is produced by a circular jet at approximately x/D=2. Gardon et al. (1962) also showed that three peaks were visible at radial displacement of 0.5, 1.4, and 2.5 nozzle diameters from the stagnation point for lower Reynolds numbers. The peak at x/D=0.5 has been explained by change in radial velocity where stagnation region ends and the wall-jet region starts. Second maxima at x/D=1.4 can be explained by a transition from laminar to turbulent boundary layer flow. Third maxima occurs at x/D=2 because this location coincides approximately with the point where toroidal vortices, which form in the shear region around the circumference of the jet, strike the plate at Z/D=1.2 and 2 (Popiel and Trass 1982). As the Reynolds number was increased to approximately 20000 the outer maxima merged and only two maxima were seen. Nusselt number profile tends to look alike a bell shaped form for Z/D>4. For Z/D values smaller than 4, vortices generated cannot penetrate because of the strong jet core. As Z/D increases, vortices coalesce and result in a peak at stagnation point.

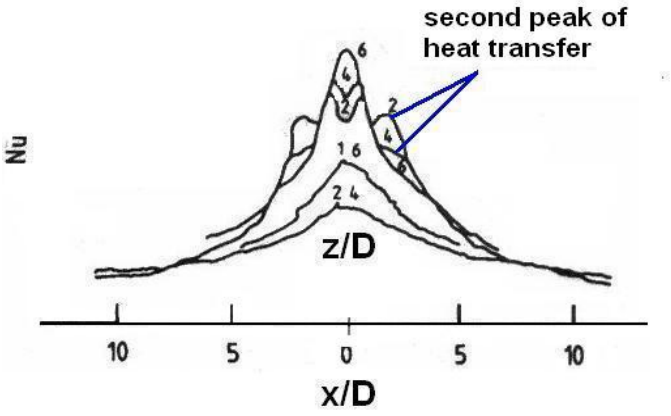

Figure 2.1. Radial variation of heat transfer coefficient
(Source: Gardon et al. 1962)

There are three reasons for the peaks in the radial distribution of heat transfer: the peak at x/D=0.5 has been explained by the change in the radial velocity, as it accelerates rapidly in the deflection region so does the shear and corresponding heat transfer.

Gardon and Akfirat (1965) suggested that the increase in the heat transfer coefficient within the range of $1 \leq x/D \leq 2$ can be explained by a transition from laminar to turbulent boundary layer flow. At a greater radial distances from the stagnation point, a fall in the heat transfer rate occurs because of the reduction in the flow velocity in the radial direction.

Results of Köseoğlu and Başkaya's studies (2010) also pointed out a similar heat transfer coefficient profile:

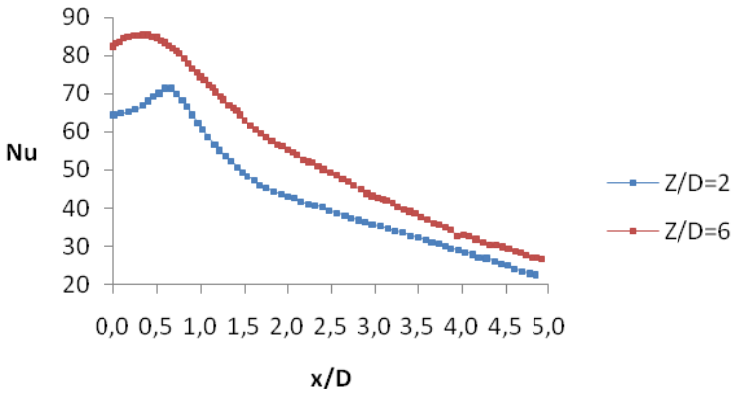

Figure 2.2. Radial variation of heat transfer coefficient
(Source: Köseoğlu and Başkaya 2010)

Popiel and Trass (1982) reported that the position of the maximum heat transfer at x/D=2 coincides with the point where toroidal vortices, which were originated in the jet shear layer, strike the plate at x/D=1.2 and 2. They also showed that the ring-shaped eddies are formed in the wall jet at the point where the toroidal vortices reach the plate. This coincidence is believed to create increased mixing in this region and therefore increase in heat transfer.

With reference to Wolf et al.'s (1993) categorization on jet impinging jet flow, it can be suggested that radial boundaries play great role on jet impingement heat transfer. Literature surveyed includes both five categories mentioned by Wolf et al, however, jet impingement setup studied in our experimental work is not investigated in detail. In the first chapter of this thesis, Wolf's categorization was discussed, concluding that our study is a combination of confined and submerged jet. This uncommon property of our experimental setup will be one of the main characteristic features that differs this study from the literature.

2.2. Effects of Confinement on Jet Flow

Confinement is another important parameter that affects impinging jet flow heat transfer characteristics. A schematic view of a submerged (unconfined) and confined jets, and the setup used in present study is given in Figure 2.3, respectively. The submerged jet is injected directly into a miscible atmosphere (liquid into liquid), and the confined jet is injected into a region bounded by the impingement surface and nozzle plate.

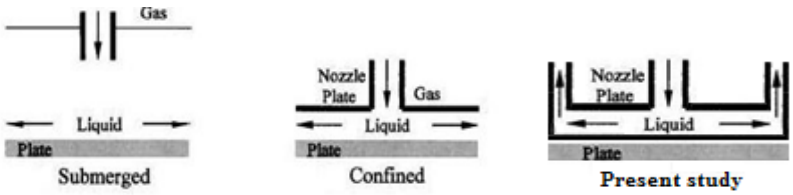

Figure 2.3. Schematic view of submerged (unconfined) and confined jets

Obot et al. (1982) showed that confinement causes a reduction in the heat transfer rate. This reduction increases with increasing flow rate. At Z/D=6 and x/D=6, a 4 percent reduction in the heat transfer due to flow confinement occurred at a Reynolds number of 29.673 and a reduction of 10 percent occurred at Re = 50.367. The data appears to show that this reduction will be least when Z/D=6.

Baydar and Ozmen's (2005) studies focusing on the flow structure and heat transfer characteristics of submerged and confined jets suggest that the effect of confinement on flow structure is significant for nozzle-to-plate spacing up to 2. Their experimental data show that, turbulence intensity along the impingement surface has two distinct peaks for both jet configurations as well. As the first peaks for both jets occur nearly in the same location, the location of second peak in submerged jet is closer to stagnation point with respect to that of confined jet, addressing a linkage between the peaks in turbulence intensity and the peaks in heat transfer coefficients on the impingement plate.

As it can be seen from the schematic view in Figure 2.3, this thesis studies a jet configuration which is a combination of submerged and confined jet.

2.3. Effects of Reynolds Number on Jet Flow

Reynolds number effect on heat transfer coefficient of an impinging jet has been studied by many researchers. A common definition of Reynods number was given in equation 1.1.

Martin (1977) showed that at Re<1000 the flow field exhibits laminar flow properties, at Re>3000 the flow has turbulent features, and a transition regions occurs between these two regimes. Turbulence has a large beneficial effect on the heat transfer rates. Martin also reported that, a round jet at Re=2000 (transition regime) and Z/D=6 resulted in an average Nusselt number of 19 over a circular target where *L/D=6*. On the other hand, at Re=100.000 the average Nusselt number on the same target reached 212. Another suggestion made by Martin is that, average Nusselt number of a laminar jet at closer target spacing (Z) at the same Prandtl number is the range of 2 to 20.

Correlations have been developed from many investigators' measurements gives the functional relationship between Nusselt, Reynolds and Prandtl numbers. One of these correlations (Martin, 1986) is given as:

$$\frac{Nu}{Pr^{0.42}} = \frac{D}{x}\frac{1-1.1\frac{D}{x}}{\left(1+0.1\left(\frac{Z}{D}-6\right)\frac{D}{x}\right)}\left[2Re^{0.5}\left(1+\frac{Re^{0.55}}{200}\right)^{0.5}\right] \tag{2.1}$$

Sagot et al. (2008) studied jet impingement heat transfer on a flat plate at a *constant wall temperature*. In accordance with their experimental data, they suggested a Nusselt number correlation for $10000 \leq Re_j \leq 30\,000$, $3 \leq L/D \leq 10$ and $2 \leq Z/D \leq 6$:

$$\overline{Nu} = 0.0603Re_j^{0.8}\left[1-0.168\left(\frac{L}{D}\right)+0.008\left(\frac{L}{D}\right)^2\right]\times\left(\frac{Z}{D}\right)^{-0.037}\left(\frac{\mu_j}{\mu_w}\right)^{0.25} \tag{2.2}$$

where $\overline{Nu}$ is surface average Nusselt number, Re_j is Reynolds number with respect to jet inlet velocity, *L/D* is dimensionless heated plate radius and *Z/D* is nozzle to plate spacing. With reference to the correlation they proposed, the authors concluded that the average Nusselt number increases with the jet Reynolds number, decreases with

the plate radius but has only a little dependency on both the nozzle-to-plate distance and fluid-to-wall temperature difference.

2.4. Effects of Nozzle Turbulence Intensity on Jet Flow

In turbulent flows, the instantaneous values vary with time, where the variations have irregular fluctuations about mean values. These fluctuations are significant and cannot be neglected. Instantaneous values can be decomposed as time averaged (mean) and fluctuating parts by the method of Reynolds decomposition as given in (2.4). Although not only velocity components, but also temperature, pressure and density components have fluctuating parts theoretically, only velocity components are given below:

$$\begin{aligned} u &= \bar{u} + u' \\ v &= \bar{v} + v' \\ w &= \bar{w} + w' \end{aligned} \tag{2.3}$$

The turbulence intensity, also often referred to as turbulence level, is defined as,

$$I = \frac{u'}{u} \tag{2.4}$$

where u' is turbulent velocity fluctuations and u is the mean velocity. Similar intensity values can be defined for each coordinate axis.

Instantaneous, mean and fluctuating velocities can be shown schematically as follows:

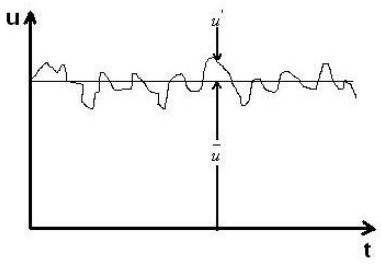

Figure 2.4. Variation of the turbulent velocity component u with time

Turbulence intensity, which has been defined above in detail, at the nozzle exit has a key role on jet flow and jet impingement heat transfer. Den Ouden and Hoogendoorn (1974) have investigated the effect of small-scale turbulence on heat transfer in impinging jet. They showed that the level of turbulence at the nozzle exit has an impact on the heat transfer at the stagnation point. For example, an increase in the axial turbulence intensity from 0.5 to 3.2 percent (at Re=60000, and Z/D=2) has resulted in an increase in the Nusselt number at the stagnation point from 180 to 215 and has eliminated the local minimum in heat transfer coefficient often seen at small nozzle to plate spacing. However, the results of Gardon and Akfirat (1965) showed that the effect of nozzle exit turbulence on heat transfer is relatively small for Z/D>6 where turbulence generated in the shear layer predominates the initial turbulence effects.

Mankbadi et al. (1989) suggested that increasing the initial turbulence was found to reduce the amplification of the fundamental component and hence lowers the spreading rate of the excited jet.

It is obvious that, acoustical actuation causes changes in fluctuating components of velocity, though mean velocity of the flow remains unchanged. In other words, actuation results in a change in turbulence intensity. Literature dealing with this effect of acoustic actuation on turbulence will be discussed under jet actuation topic.

2.5. Effects of Nozzle Geometry on Jet Flow

Nozzle geometry is a dominating factor which extensively affects heat transfer characteristics of an impinging jet flow. Since the initial turbulence intensity of flow strongly depends on nozzle geometry, it has been considered worth studying by many investigators.

Obot et al. (1982) suggested that variation in turbulence levels due to different nozzle designs causes variation in measured heat transfer rate, particularly in the optimal nozzle-to-plate spacing for maximum heat transfer. For a nozzle with a sharp-edged inlet and a length-to-diameter ratio of 1 (Re = 29.485) the maximum stagnation point Nu number of 155, occurs at z/D = 4, and with a contoured inlet the maximum, Nu = 125, occurs at z/D = 8.

Popiel and Boguslawski (1988) showed that the area mean heat transfer due to an impinging jet issuing from a contoured nozzle is 25 percent less than that of a jet

from a sharp-edged orifice when z/D = 4, Re = 20000, and x/D = 1. The effect of nozzle geometry on heat transfer is most significant in the region near the stagnation point.

Gundappa et al. (1989), who compared the axial velocity decay and the impingement heat transfer due to orifice jets and to jets issuing from pipes (Pipe length/D = 10), showed that the axial velocity was seen to decay more slowly in the case of the jet produced by the pipe. Gundappa et al. suggested that this led to the higher values of Nusselt number seen for the impinging pipe jet at all radial positions when z/D=7.8. At smaller nozzle-to-plate spacings the different nozzle designs were seen to produce differing shapes of radial Nusselt number distribution.

Jambunathan et al. (1992) discussed the effect of nozzle geometry in their review paper. They concluded that for nozzle-to-plate spacing less than Z/D=10, the use of an orifice should cause higher rates of heat transfer than a contoured nozzle. Turbulence generating effect of nozzle geometry in the shear layer is the main reason that leads them to this conclusion.

Çelik and Eren (2009) investigated the heat transfer performance of co-axial jets, showing that for d/D=0 (where d is outer diameter of inner tube and D is inner diameter of outer pipe), which corresponds to a singular round jet, the heat transfer coefficient is at least. They suggested that, heat transfer coefficient makes a maximum for d/D=0.55.

Köseoğlu and Başkaya (2010) studied the effects of nozzle geometry on impinging jet heat transfer. They concluded that, wall jet region comprises very large portion of the impinging plate and generally lower heat transfer rates were attained for higher aspect ratio jets in this region especially at small jet to plate distances, where aspect ratios of the jets were defined as the ratio of major axis length to minor axis length. They suggested that, the effect of aspect ratio on local and average heat transfer decreases with increasing jet to plate distance. Their studies showed that, with increasing jet to plate distance, the differences between the heat transfer characteristics of the major and the minor axis almost disappeared and very similar heat transfer characteristics were observed along the major and minor axis directions.

2.6. Jet Actuation

Although the first jet acoustics investigators' aim was determining the dominating factors that causes noise in jet flow, since it has been understood that acoustic disturbance creates an opportunity on controlling the characteristics of large

and small scale motions, jet researchers have focused their research studies on this topic. In their study on direct excitation of small-scale motions in free shear flows, Wiltse and Glezer (1998) noted that "mixing processes in turbulent shear flows are induced by a hierarchy of vortical structures of decreasing scales coupled by local cascade of momentum and energy until molecular mixing ultimately takes place at the smallest scales. These vortical structures evolve as a result of inherent hydrodynamic instabilities of the base flow and, at least within a limited band of wavelengths, can be manipulated through the introduction of controlled disturbances at the flow boundary." In accordance with this phenomenon, acoustic jet actuation is used to control flow instabilities, for the purpose of enhancement of mixing in chemical processes, heat transfer, or plume reduction.

Jet actuation occurs when a perturbation alters the instabilities in the shear layer between the jet and the ambient medium. There may be some cases which will push the investigator to introduce artificial actuation, such as enhancement of mixing and concludingly heat transfer in impinging jet flow. The actuation amplifies the structures of interest and locks them into a regular frequency. It should be noted that, the investigator has to avoid from the risk that artificial actuation may suppress the turbulence in a free shear flow, which may result an unwanted effect and even decrease the impinging jet's heat transfer coefficient, as it was pointed out at Hwang et al.'s studies (2003). In their experimental reports, it is noted that, for the case of St=2.4, the vortex pairing is suppressed and the development of jet flow is delayed resulting in the longer potential core length with lower turbulence intensity. They showed that heat transfer rates are reduced at smaller nozzle-to-plate spacing values and the formation of the secondary peak of the heat transfer coefficients is delayed due to the low turbulence intensity of the jet core flow.

Clifford (2005) addresses to the fact that, the boundary layer between two fluids with different velocities, temperatures, and densities is naturally unstable. As the fluids mix in search of equilibrium, the boundary layer expands forming Kelvin-Helmholtz instability waves. As the instability waves grow, they break down and dissipate leaving the fluid fully mixed in equilibrium.

Hussain and Zaman (1981) noted that phase-locked coherent structures do not occur beyond 6 jet diameter downstream of the nozzle exit ($z>6D$). Turbulence intensity in the actuated and normal jets is also the same between six and eight jet diameters along the z-direction. It is thought that the turbulent structures lose their identity beyond

these values, leading us not to exceed the nozzle-to-plate spacing of 6, in our experimental studies.

The behavior of the instability waves may be decomposed into modes of oscillation for the convenience of the analysis. Each mode is characterized by an initial growth rate. Additionally, each mode has a preferred frequency or its non-dimensionless form is Strouhal number where maximum amplitude may be obtained. Crow and Champagne (1971) found that the mode with maximum amplitude at the end of the potential core corresponds to the mode with Strouhal number is equal to 0.3.

Raman, Zaman and Rice (1989) show that jet whose initial turbulence intensity varied from 0.15 to 0.5 percent responded to the excitation. In accordance with their experiments, they suggested that at all initial turbulence levels responded to the excitation; the amplitude required reaching the same level of response, however, increased as the initial turbulence intensity increased.

Mankbadi, Raman and Rice (1989) varied only the core turbulence intensity while holding the turbulence intensity in the boundary layer as steady as possible. They found that the jet response was reduced as core turbulence intensity increased. Thus more turbulent flows require more powerful actuators to excite them.

Wiltse and Glezer (1992) studied excited air jet by using four piezoelectric actuators placed along the sides of the square jet nozzle exit. They show that at low excitation levels, the flow is not receptive to excitation and induced velocity perturbations are rapidly decreased. Although the amplitude of the actuator displacement is less than one millimeter, the magnitude of the induced velocity perturbation is proportional to the product of the actuator displacement and its frequency. Hence, if the frequency is high enough, the induced velocity perturbation can be quite large and lead to roll up of line vortices. Farther downstream from the actuators, the line vortices coalesce and rapidly lose their identity. Nevertheless the formation of these vortices is accompanied by a considerable increase in the cross-stream spreading of the jet shear layer. Hence excitation at frequency with non-uniform amplitude distribution can result in a substantially distorted mean flow.

Wiltse and Glezer (1998) also focus on direct excitation of the small scales within the dissipation range of a free shear flow. They noted that high frequency excitation significantly enhances the turbulent dissipation. Even though the excitation does not alter the mean distribution of the velocity fluctuations within the domain, the dissipation in the forced flow increases relatively to the unforced flow. A small increase

in velocity perturbations at high frequencies can lead to significant enhancement of the dissipation and to a decrease in the turbulent kinetic energy within the jet shear layer.

Hwang et al. (2003) reported that, for St=1.2, the jet flow has a shorter potential core length and a slightly higher turbulence intensity than that of the non-excited jet. Their experiments showed that as the jet flow is acoustically actuated by St=1.2, the heat transfer rates are enhanced a little at the small nozzle-to-plate spacing because of the high turbulence intensity at the nozzle exit. They also suggested that, for the acoustic actuation of St =2.4, the heat transfer rates are reduced a little for small nozzle-to-plate spacing and the formation of the secondary peak of the heat transfer coefficients is delayed due to the low turbulence intensity of the jet core flow.

Hwang et al. (2003) have also actuated impinging jet flow both from upstream end and from the nozzle exit. Their experiments show that though the position of jet actuators is different, flow characteristics and obtained heat transfer coefficients of both configurations did not differ at all, moreover, they give nearly same results for both cases.

Zhou et al. (2004) have studied the effect of positioning a mesh screen upstream of a jet impingement setup. They showed that heat transfer increases moderately up to Z/D=4, pointing out that this enhancement is attributed to the increased turbulence within the potential core.

Bhattacharya et al. (2010) have focused on a more direct actuation method. They placed a stationary cylinder, an eccentrically mounted cylinder and an airfoil in the downstream of an impinging jet, letting them rotate around a pin which fixes them to the assembly. The ensuing oscillating jet configurations showed higher heat transfer rates than non-actuated jet tested under the similar conditions. The improved heat transfer characteristics were attributed to two mechanisms consisting of enhanced mixing/turbulence due to bluff body wakes vortex dynamics and oscillatory dislocation of the stagnation streamline.

2.6.1. Types of Flow Actuators

A brief summary of flow actuators which are commonly used in jet actuation and mentioned in cited literature is summarized below.

Flow actuators generate forces that act on the flow and create the excitation effect. Depending on the actuator, the forces generated may assume different forms. A

typical classification is suggested by Clifford (2005) as physical, pressure (acoustic) based and fluidic actuators (Figure 2.2). It is obvious that, each method has advantages and disadvantages.

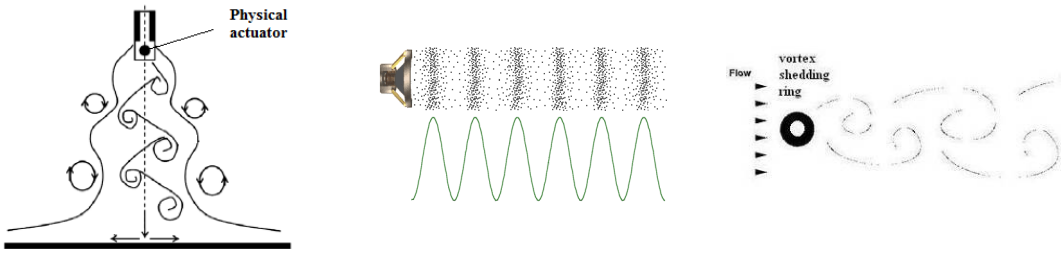

(a) Physical (b) Pressure based (c) Fluidic

Figure 2.5. Types of flow actuators

The simplest excitation method is by a physical actuator. Typically, a solid body is placed in the flow to influence its behavior. Physical actuators redirect the flow and change the amplitude of the instability waves. This simple technique has promise in mixing applications with minimum external energy input. However, their frequency response is often limited. Common types of the physical actuators are stationary or oscillating bodies, vibrating ribbons, thin flap and piezoelectric actuators such as shown in Figure 2.5.a.

Most commonly used pressure based actuators are sound waves. Mostly this actuation type is generated by a loudspeaker as it is demonstrated in Figure 2.5.b. A loudspeaker has several advantages for excitations; they are cheap, strong and easily controllable in frequency and in amplitude. While this makes them a convenient tool, there are limitations on the maximum wave amplitude and frequency that may be generated, restricting the size and speed of the jet that may be influenced. In addition, their size and weight make loudspeakers a poor choice for any application that requires mobility. They have been used in this study for their cheapness and convenient features for laboratory works.

Last actuator type is fluidic actuators. This kind of actuators acts on the flow in the form of pulses or vortices. Its main objective is to generate these structures in the flow naturally and utilize its actuation effects. A simple example consists of a vortex shedding ring as shown in Figure 2.5.c, placed nearly upstream of the nozzle exit where the fluids generate exciting vortices. The frequency of the vortex generation is

controlled by the diameter of the ring. Its main difference from the mechanical actuators is to utilize the vortex generation instead of redirection of flow by solid barrier for actuation. Another example is studied by Bhattacharya et al. (2010): a cylinder with a pin located at 2.5 mm from the center allowing the cylinder to oscillate when positioned in the jet is used as a fluidic actuator.

Flip-flap actuators are used as fluidic actuators too. A flip-flap actuator includes no moving parts but the geometry itself is considered as an actuator. The nozzle geometry causes vortices in the fluid, and the interacting vortices and consequent pressure differences in the fluid result in oscillations in the liquid jet at the nozzle exit.

Synthetic jet, which was introduced in the first chapter of this thesis, is also a kind of fluidic actuator. As it was mentioned before, the mechanism moves a membrane or diaphragm up and down hundreds of times per second, sucking the surrounding fluid into a chamber and then expelling it. Although the mechanism is fairly simple, extremely fast cycling requires high-level of engineering to produce a device that will last in an industrial applications.

An example to a new generation fluidic actuators is a spark driven actuator. They excite the flow by a rapid expansion of fluid due to a combustion process or due to temperature expansion. Obviously these actuators cannot be employed for liquid-to-liquid jets. They are also limited by a frequency response because of the total time required to complete burning process. Its advantages are opportunity of high amplitude and high frequency force for high Reynolds number flows.

CHAPTER 3

EXPERIMENTAL SET UP

3.1. Jet Parameters of Experimental Setup

A jet impingement setup is built aiming to study the effects of nozzle-to-plate spacing, nozzle geometry, radial distance from the jet center and frequency and waveform of actuation waves including all auxiliary measuring rigs. A 3-D solid design software is used as a design tool during various design steps. Related analysis and material selections are presented in the following. It must be noted that this setup was first built by Bilgin (2009) and many details were given in his theses. Our work has been a continuation of his design and many parts were built on top of it and therefore helped us to save considerable time.

Determination of jet impingement parameters affects the basic dimensions of the experiment set-up. Parameters are the ratio of radial distance from jet nozzle axis to the diameter of jet (X/D), the ratio of axial distance from nozzle exit to impingement plate to jet diameter which is so called nozzle-to-plate spacing (Z/D), Reynolds and Strouhal numbers.

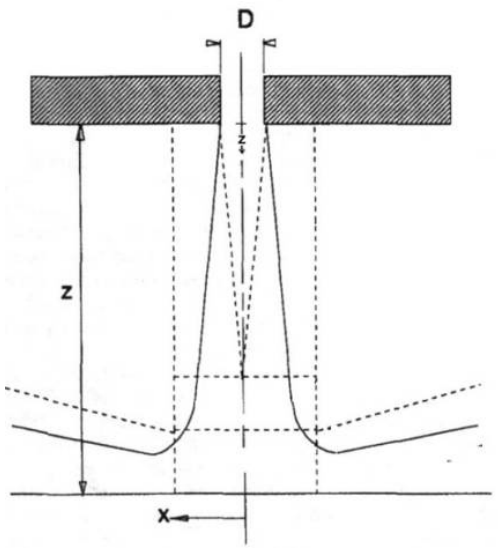

Figure 3.1. Jet parameters

Deciding the radial and axial dimensions of the setup (X and Z) is accomplished by researching their effects on the jet. It can be seen that for radial distance X greater than about 7 nozzle diameters, the local heat transfer coefficient is independent of the nozzle to plate spacing (Z) as seen in Figure 3.2 (Gardon et al. 1962). For this reason, X is chosen to be greater or at least equal to 7 nozzle diameters. Suitable range for Z/D ratio is chosen such that the interesting second peak of heat transfer coefficient as shown in Figure 3.2 can be observed; therefore this ratio is chosen between 2 to 6. The nozzle diameter is assigned to be 5 mm.

It should be noted that, values suggested by mentioned literature deals with confined or in-line jets, which are somewhat different from present study. As it was mentioned in literature survey, our experimental setup is not only confined by the plate where the jet exits, but also confined by walls placed at both sides. This feature of our setup is thought to be as a significant parameter that differentiates the present study from the literature.

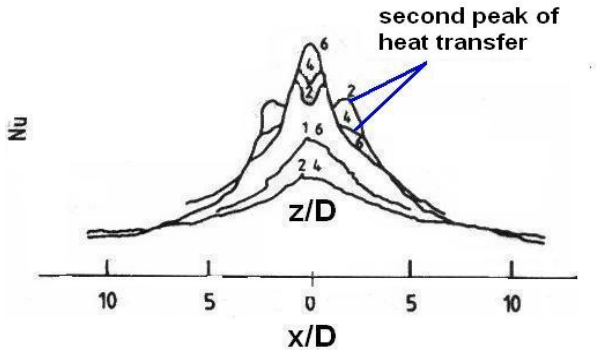

Figure 3.2. Effects of jet parameters on heat transfer coefficient
(Source: Gardon et al. 1962)

Briefly, the reservoir of the jet is X/D≈36x36 (180 mm * 180 mm) for the sudden contracting nozzle. Smooth contracting nozzle is produced such that, the curvature of the contraction is a fifth degree polynomial, which can be formulated as,

$$y = -1.4\times10^{-7}x^5 + 2.32\times10^{-5}x^4 - 9.9\times10^{-4}x^3 - 2.5 \qquad (3.1)$$

This kind of a contraction provides us a jet inlet velocity profile that is almost free from the turbulent fluctuations those of which are originating from the uncontrolled factors present in upstream of the setup or the natural instabilities of the jet flow itself. Technical drawings of investigated nozzle geometries can be seen in Figure 3.3. Both nozzles can be unassembled and mounted back again easily.

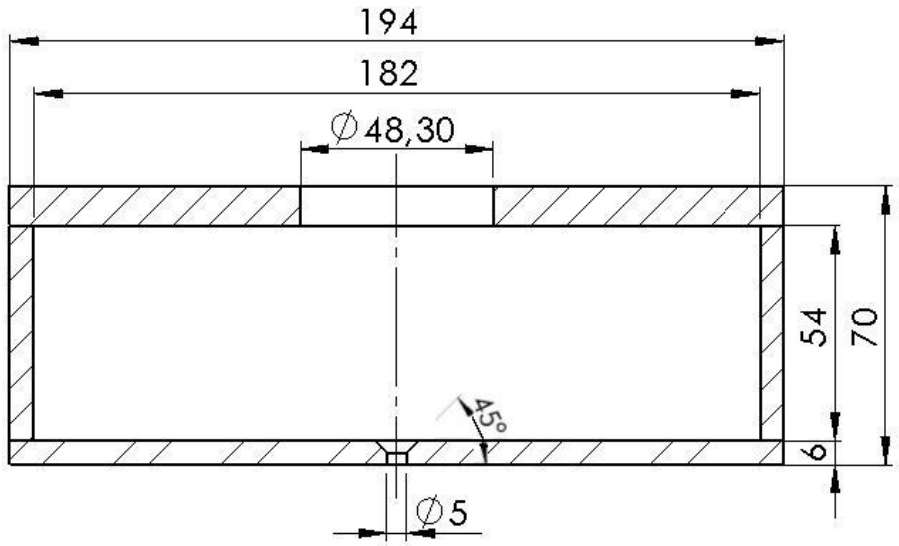

(a) Sudden contracting nozzle (5 mm diameter) and the standpipe

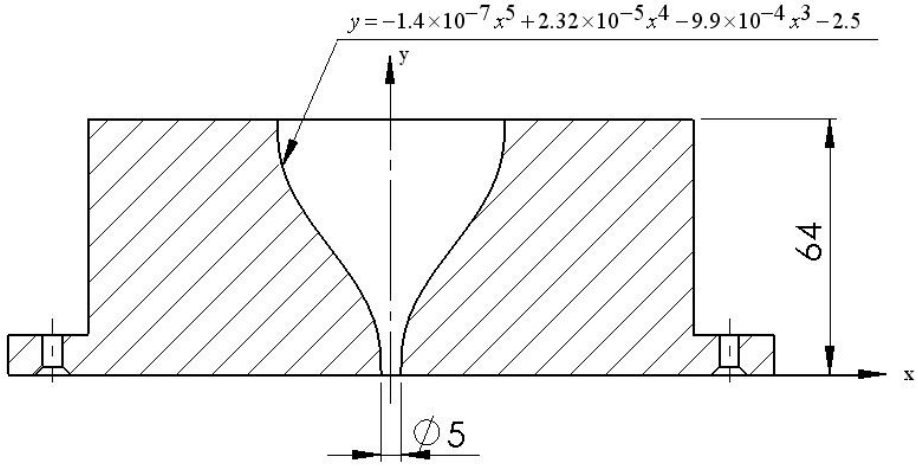

(b) Smooth contracting nozzle (5 mm diameter)

Figure 3.3. Investigated nozzle geometries

Since turbulence increases the mixing of the coolant fluid, it leads to an enhancement in the heat transfer coefficient. Therefore effective management of turbulence in the jet results in higher heat transfer. This fact motivated us to investigate the flow in a turbulent region, where Reynolds number is kept constant at 10000, since the main aim of this study is to shed light not onto the effects of Reynolds number, but to understand the effect of acoustic actuation on flow structures in a turbulent jet flow. This contributes to a jet exit velocity of about 2 m/s. Because of its high specific heat and thermal conductivity, water is chosen as a coolant.

3.2. Working Principles of the Experimental Setup

Confined-submerged jet is studied in the scope of this work, because of its effective heat transfer performance in a compact jet design.

A standpipe, with a honey-comb at its downstream end, is used for the regulation of the flow upstream of the nozzle. This mechanism also provides an uniform jet exit velocity profile, and it suppresses the swirl of the fluid. Flow is taken away from the test section by means of a 3 mm wide peripheral gap between the standpipe and the jet room (Figure 3.4). As soon as the fluid is taken away from the test section, it is sent back to the supply tank (for heat transfer experiments) or drainage (for flow visualization experiments). The velocity of the flow at the outflow gap is found to be very low (0-0.07 m/s) by computational fluid dynamics analysis at Bilgin's (2009) previous studies. This low velocity outlet flow ensures that almost no disturbance could occur along this path and the fluid is taken out symmetrically. The nearly symmetrical structure of the impinging jet flow can also be seen in Figure 3.5, where a flow visualization image is given.

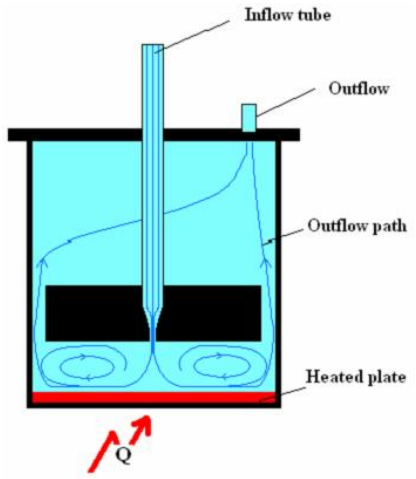

Figure 3.4. Schematic side view of the jet set-up (Smooth contracting nozzle)

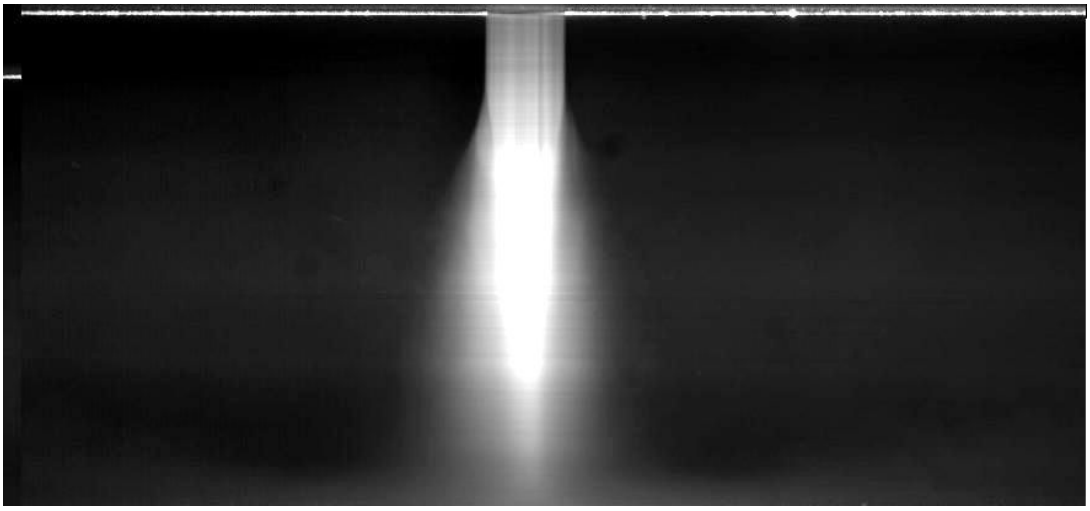

Figure 3.5. Flow visualization: a typical impinging jet flow.

For a better understanding, an artistic view of the standpipe and jet test section is given in Figure 3.6.a and b. Centering of the standpipe is provided by means of plastic L-shaped profiles placed at the corners between the jet room and standpipe. To summarize, the standpipe divides the jet room into two regions as active jet region and passive outflow region.

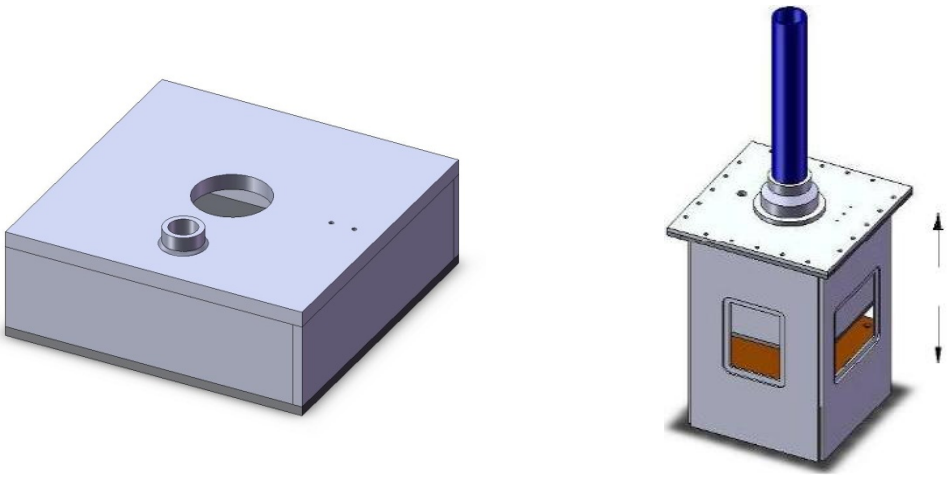

(a) Sudden contracting nozzle and standpipe **(b)** Position of standpipe in the setup

Figure 3.6. Design of the standpipe and nozzle

Section view of whole test section is given in Figure 3.7.a and b, where the nozzle-to-plate spacing (Z/D) is 2 and 6, respectively. It should be said that, nozzle-to-plate spacing is adjustable in the range of 0 and 10. As it was mentioned in literature survey, Z/D values above 6 are not investigated in this study, thus, experiments are performed for Z/D=2, 4 and 6. L/D, which is dimensionless for of heater surface length, is taken as 40 (= *200 mm*) for all experiments.

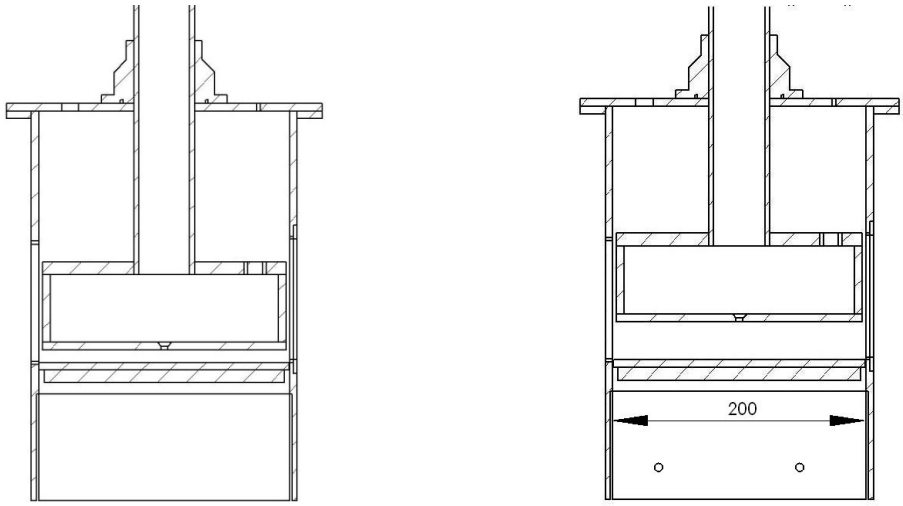

(a) Z / D = 2 **(b)** Z / D = 6

Figure 3.7. Adjustment of Z/D by traversing the standpipe

3.3. Experiments with Water Jet

Water is used as coolant in all experiments. A schematic view of the experimental setup for water jet is shown in Figure 3.8:

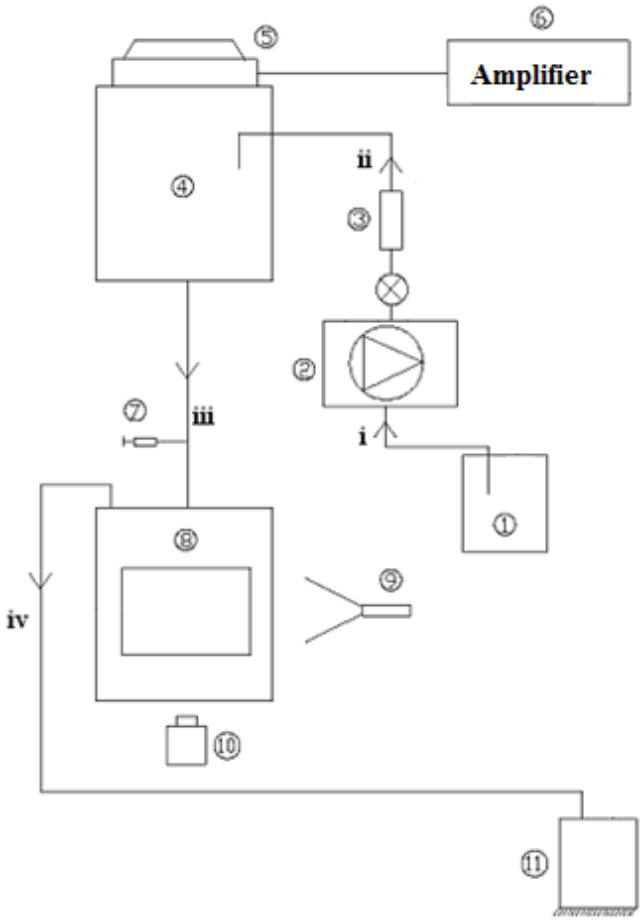

1. Supply Tank
2. Pump
3. Flow meter
4. Water tank
5. Loudspeaker
6. Amplifier and cold plate
7. Red food-dye Injection
8. Jet setup
9. Laser
10. CCD camera
11. Drainage
i. Supplying pump line
ii. Supplying water tank line
iii. Jet supplying system line (in)
iv. Jet supplying system line (out)

Figure 3.8. Experimental setup for water jet

The jet velocity of 2 m/s is provided by free fall of the water which is collected in a container mounted on the wall. Jet velocity is kept constant by keeping the height of the free surface of water column steady in the water tank (4). Required water is provided from supply tank (1) by a centrifugal pump (2). While flow visualization experiments are running, the water is emptied to drainage (11) to keep the system clean from flow marker (regular red food-dye – *Rhodemin B* - for this case).

The description of the flow diagram is as follows: Water taken from the supply tank by the supply line (i) is pumped by a centrifugal pump to the water tank, through line (ii). The fluid passes through a flow meter (3) and reaches to the water tank as it

supplies water directly to the jet set-up (8). Another line is for the cold plate of the loudspeaker amplifier (6) to cool its electronics which is carried a the line that is not figured in the flow scheme. Water is actuated by sound waves from a loudspeaker (5) which is then transmitted to the jet set-up by the line (ii). Red food-dye (*Rhodemin B*), which is used as a flow marker for flow visualization purposes, is injected to the flow by an injection apparatus (7). Later on, actuated water jet impinges to the plate, and leaves the test section through the line (iv) to the drainage (11).

A power laser (9) is used to illuminate the cross section of the jet nozzle (usually the center plane). A CCD camera (10) which is directed on the illuminated plane acquires images of the jet flow. Captured images are either used as it is (instantaneous) or averaged pixel by pixel to obtain a more general picture. A high speed camera is also used for visualization purposes. Those images captured the high speed camera gives us very clear and valuable results which leads us to comment on roll-up events in the jet flow.

Supply tank (Figure 3.9) is used for storing enough clean water for the experiments. There are three filters installed on supply tank to keep the water clean. Free fall of the water for obtaining constant jet inlet velocity is initiated in the water tank (Figure 3.10). The steadiness of the free surface of the water was observed for at least 5 minutes before running each experiment.

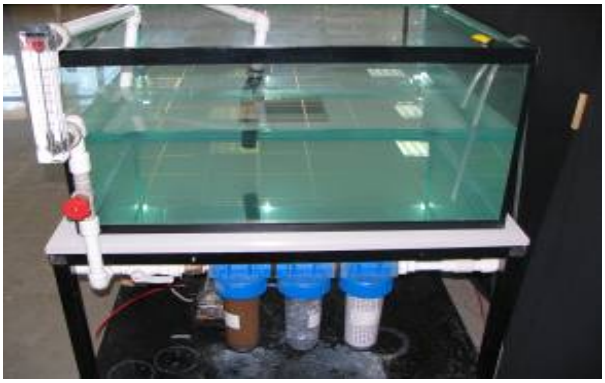

Figure 3.9. Supply Tank

Figure 3.10. Water Tank

The loudspeaker mounted on top of the water tank generates sound pressure waves above the water tank where it can be seen in the Figure 3.10 and 3.11. It is 11'' inches in diameter and has a working range of 25 Hz-2500 Hz with total of 450 W. The loudspeaker is controlled by an amplifier, which can be seen in Figure 3.12. It is fed by

sinusoidal or square waves by a function generator seen in Figure 3.13. Since the amplifier circuit needs to be cooled down rigorously, a water-cooled cold plate is assembled under it. It should be noted that, Strouhal number is adjusted by changing the actuation frequency (f), while other variables such as jet inlet velocity (V) and jet diameter (D) are kept constant.

Figure 3.11. Loudspeakter: 11'' diameter, 450 W

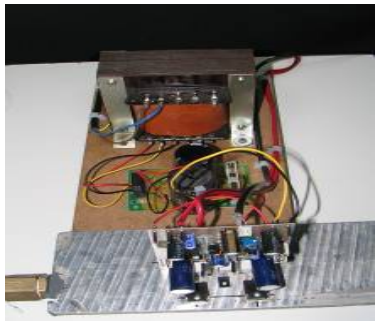

Figure 3.12. The amplifier

Figure 3.13. Function generator, power supply, oscilloscope, computer

In flow visualization experiments, cross section of the jet is illuminated by a laser sheet. Laser beam is sent through a cylindrical lens to create a light sheet to illuminate a planar 2D section of the flow which passes through the jet center. The alignment of laser beam and cylindrical lens is provided by means of a laser sheet rig which is designed and manufactured by us. Laser sheet rig mechanism can be seen in Figure 3.14.a and 3.14.b. The laser sheet rig is designed such that the laser beam can be perfectly aimed on the cylindrical lens which is able to turn around itself. This feature of laser sheet rig provides us the ability of perfectly align of the laser beam and the lens so that a perpendicular and a symmetric laser sheet is obtained.

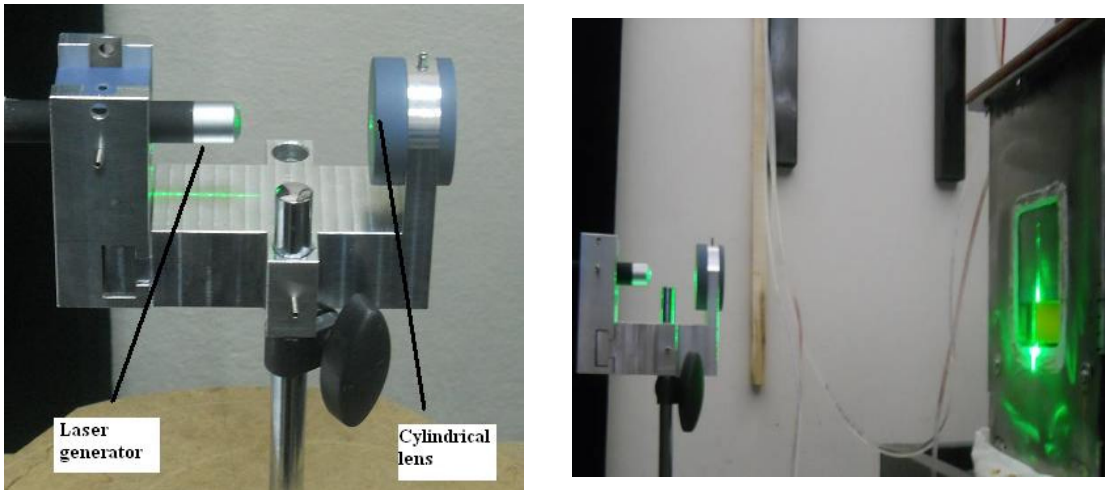

(a) Laser sheet rig **(b)** Cross section illumination

Figure 3.14. Laser sheet rig and cross section illumination

3.4. Heater Assembly and Heat Transfer Coefficient Measurements

Constant heat flux is applied to the impingement plate, which is made up of copper. Back of the heating plate is covered with an insulating material to minimize the heat loss. Temperature measurements were made by J-type thermocouples. The copper plate is drilled with 1 mm drill bit just 1 mm next to the wet surface of the copper plate so that the wetted surface's true temperature and the thermocouple temperature is almost the same (Figure 3.15).

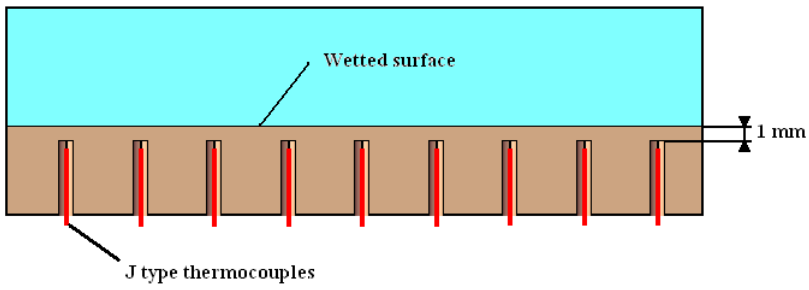

Figure. 3.15. Thermocouple assembly

Jet is impinged on the upper part of the copper plate. Bilgin's studies were focusing on a circular heat source that has a smaller area but a higher heat flux in the

stagnation region. In this study, the impingement plate is heated as a whole which gave us the opportunity of analyzing not only the stagnation region measurements, but also the wall jet region temperature values. Because of limited technical facilities, the heat flux is reduced with respect to Bilgin's previous work due to the widening of heated area, as the heating power fed into the system is almost the same.

Required heat flux is provided by a resistance wire which provides 1020 W of heating power, and temperature distribution over the heated plate is measured by 12 thermocouples that are positioned on the centerline of the copper carrier. Those are located at x/D=0, 0.5, 1, 1.5, 2.5, 3, 3.5, 4, 4.5, 7, 10 and 15 as it can be seen in Figure 3.16. Another thermocouple is also used for measuring the inlet water temperature.

The copper (Cu) plate whose conductivity is about 380-401 W/mK with an area of 400 cm^2 is heated by a wire resistance whose power is approximately 1020 W. This corresponds to a uniform heat flux of 2.55 W/cm^2.

$$q'' = \frac{Q}{A} = \frac{1020}{400} = 2.5 \text{ W/cm}^2 \tag{3.1}$$

The copper plate has a thickness of 10 mm, to provide a uniform heat flux in the axial direction. This thickness is thought to be enough for uniformity, on the other hand, when the coolant fluid is impinged on the heated surface, center of the plate cools down more, which will result in a conductive heat transfer from the outer and hotter regions of the plate to the center. The occurrence of this radial heat transfer is an unwanted situation, so the effect of radial heat transfer with respect to axial heat transfer is investigated, in our preliminary experiments, where,

$$Q_R = -k\, A_{cr} \frac{dT}{dx}\Big|_{x_1}^{x_2} = -k 2\pi r H \frac{dT}{dx}\Big|_{x_1}^{x_2} \tag{3.2}$$

Here, k is conductive heat transfer coefficient and A_{cr} is the cross sectional area. The physical meaning of equation 3.1 can be seen in Figure 3.17, where a small section view of the heated plate is plotted. x=0 is the center of the copper plate. H is the thickness of the plate.

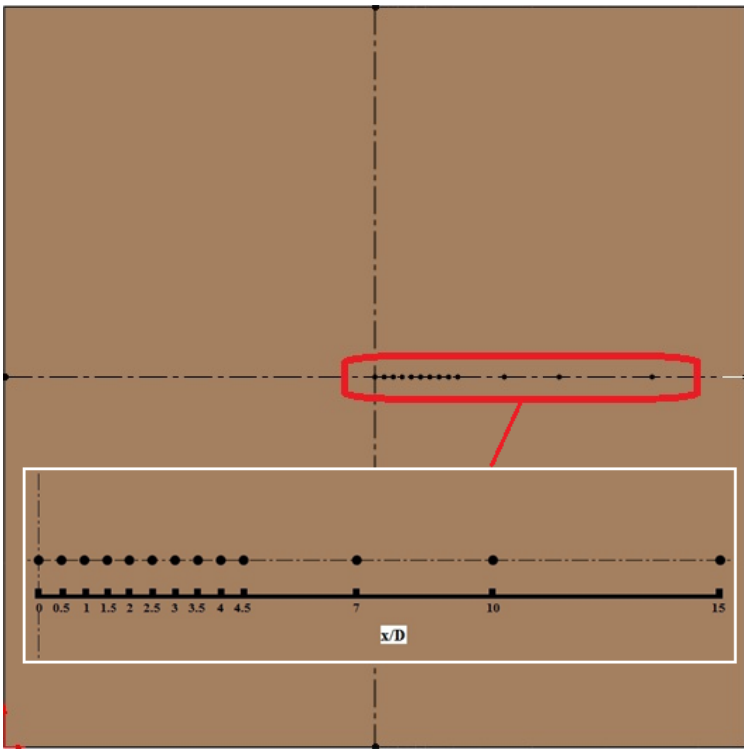

Figure. 3.16. Radial position of thermocouples

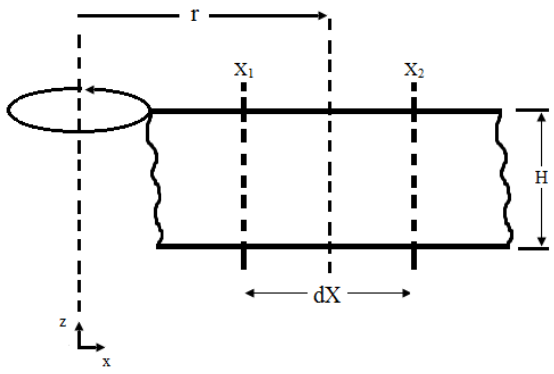

Figure. 3.17. Physical meaning of equation (3.1)

The measured surface temperature and the inlet temperature for any case are used for calculation of convective heat transfer coefficient *h* and therefore the Nusselt number *Nu* of the convective heat transfer, as:

$$h = \frac{Q_{net}}{A\Delta T} \tag{3.2}$$

$$Nu = \frac{hD}{k_w} \tag{3.3}$$

Where, Q_{net} = Q_{total} - Q_{loses} and A is the surface area of the heated area and ΔT is the difference between surface temperature and inlet water temperature, and D is the diameter of the jet nozzle.

The radial heat transfer from any data point, to its adjacent data points are calculated with the temperature distribution data given in Figure 3.18. The ratio of radial heat transfer with respect to axial heat transfer is plotted in Figure 3.19, where it can be seen that the heat applied to the test section mostly flows in axial direction, and the effect of conductive heat transfer in radial direction is negligible.

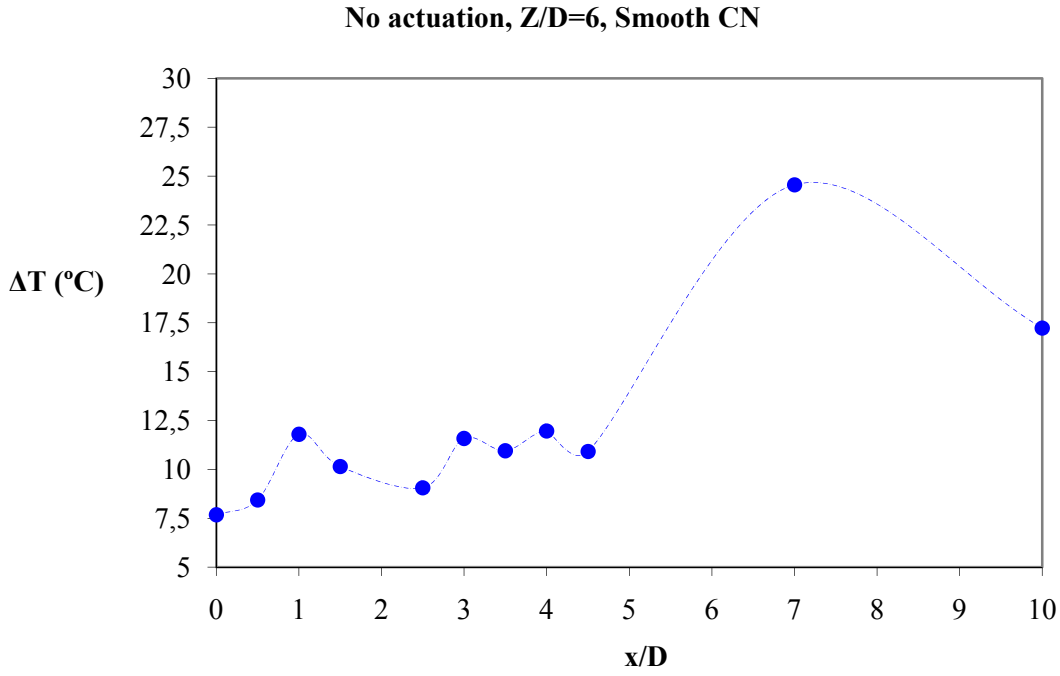

Figure. 3.18. Temperature distribution over the heated plate

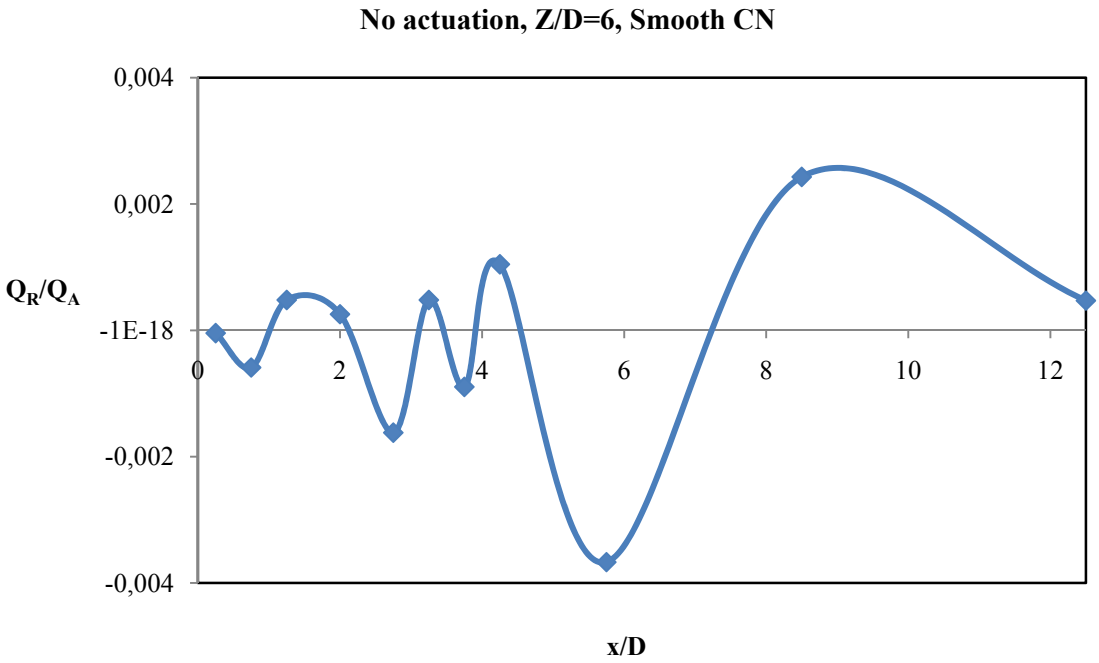

Figure. 3.19. The effect of radial heat transfer with respect to axial het transfer

CHAPTER 4

RESULTS AND DISCUSSION

4.1. Uncertainty Analysis of Experimental Results

In physical experiments, uncertainty analysis deals with assessing the uncertainty in a measurement. An experiment designed to determine an effect, demonstrate a law, or estimate the numerical value of a physical variable will be affected by errors due to instrumentation, methodology, presence of confounding effects and so on. Moreover, results of experiments often are used for engineering analysis and design. Not all data are equally good; the validity of data should be documented before test results are used for design. Uncertainty analysis is the procedure used to quantify data validity and accuracy.

Before we demonstrate the uncertainty calculations in our experiment, this is a good point to make some definitions of terms that are often misused or mistaken for one other.

They are accuracy, precision, random error, bias (or systematic) error and uncertainty (JCGM, 2008).

Accuracy: Closeness of computations or estimates to the exact or true values that the statistics were intended to measure.

Precision: The property of the set of measurements of being very reproducible or of an estimate of having small random error of estimation.

Random error: It presumably arises from unpredictable or stochastic temporal and spatial variations of influence quantities. The effects of such variations give rise to variations in repeated observations of the measured quantity.

Bias error (or systematic error): Like random error, cannot be eliminated but it too can often be reduced. If a systematic error arises from a recognized effect of an influence quantity on a measurement result, the effect can be quantified and, if it is significant in size relative to the required accuracy of the measurement, a correction or correction factor can be applied to compensate for the effect.

Uncertainty: The uncertainty of the result of a measurement reflects the lack of exact knowledge of the value of the measured quantity. The result of a measurement

after correction for recognized systematic effects is still only an estimate of the value of the measured quantity because of the uncertainty arising from random effects and from imperfect correction of the result for systematic effects.

4.1.1. Mathematical Background

Let's assume R is a function of x_1, x_2, …, x_n . The effect on R of an error measuring an individual x_i may be estimated by analogy to the derivative of a function. A variation, δx_i in x_i would cause R to vary according to

$$\delta R_i = \frac{\partial R}{\partial x_i} \delta x_i \tag{4.1}$$

For applications, it's convenient to normalize equation (4.1) with R so that we can talk about relative uncertainties:

$$\frac{\delta R_i}{R} = \frac{1}{R} \frac{\partial R}{\partial x_i} \delta x_i = \frac{x_i}{R} \frac{\partial R}{\partial x_i} \frac{\partial x_i}{x_i} \tag{4.2}$$

Here, $\frac{\partial x_i}{x_i}$ gives the uncertainty due to variations in x_i, where ∂x_i is the accuracy of measurement and x_i is the measured data itself. Hence, equation (4.2) comes out to the form of:

$$u_{R_i} = \frac{x_i}{R} \frac{\partial R}{\partial x_i} u_{x_i} \tag{4.3}$$

The combined effect of uncertainty intervals in all x_i's should be taken into account. For this purpose, the best representation which includes the effects of all errors is suggested by Kline et al. (1953) assuming that there is no correlation between the parameters:

$$u_R = \pm\left[\left(\frac{x_1}{R}\frac{\partial R}{\partial x_1}u_1\right)^2 + \left(\frac{x_2}{R}\frac{\partial R}{\partial x_2}u_2\right)^2 + \ldots + \left(\frac{x_n}{R}\frac{\partial R}{\partial x_n}u_n\right)^2\right]^{1/2} \tag{4.4}$$

4.1.2. Application to Data

Equations mentioned above are applied to decide the uncertainty of dimensionless Reynolds and Nusselt numbers since those are the key parameters that govern our experiments.

Reynolds and Nusselt numbers are both functions of many other parameters. Mainly,

$$\mathrm{Re} = \frac{4\dot{\forall}}{\pi D\nu} \tag{4.5}$$

$$Nu = \frac{hD}{k} \tag{4.6}$$

Now, let's substitute equation (4.5) into (4.4):

$$u_{\mathrm{Re}} = \pm\left[\left(\frac{\dot{\forall}}{\mathrm{Re}}\frac{\partial \mathrm{Re}}{\partial \dot{\forall}}u_{\dot{\forall}}\right)^2 + \left(\frac{\nu}{\mathrm{Re}}\frac{\partial \mathrm{Re}}{\partial \nu}u_{\nu}\right)^2 + \left(\frac{D}{\mathrm{Re}}\frac{\partial \mathrm{Re}}{\partial D}u_D\right)^2\right]^{1/2}$$

$$\frac{\dot{\forall}}{\mathrm{Re}}\frac{\partial \mathrm{Re}}{\partial \dot{\forall}} = \frac{\dot{\forall}}{\mathrm{Re}}\frac{4}{\pi D\nu} = 1$$

$$\frac{\nu}{\mathrm{Re}}\frac{\partial \mathrm{Re}}{\partial \nu} = \frac{\nu}{\mathrm{Re}}\frac{4\dot{\forall}}{\pi D}\left(-\frac{1}{\nu^2}\right) = -1$$

$$\frac{D}{\mathrm{Re}}\frac{\partial \mathrm{Re}}{\partial D} = \frac{D}{\mathrm{Re}}\frac{4\dot{\forall}}{\pi \nu}\left(-\frac{1}{D^2}\right) = -1$$

$$u_{\mathrm{Re}} = \pm\left\{\left[(1).\pm u_{\dot{\forall}}\right]^2 + \left[(-1).\pm u_{\nu}\right]^2 + \left[(-1).\pm u_D\right]^2\right\}^{1/2}$$

Similarly, uncertainty of Nusselt number can be obtained by substituting equation (4.6) into (4.4):

$$u_{Nu} = \pm\left[\left(\frac{h}{Nu}\frac{\partial Nu}{\partial h}u_h\right)^2 + \left(\frac{D}{Nu}\frac{\partial Nu}{\partial D}u_D\right)^2 + \left(\frac{k}{Nu}\frac{\partial Nu}{\partial k}u_k\right)^2\right]^{1/2}$$

$$\frac{h}{Nu}\frac{\partial Nu}{\partial h} = \frac{h}{Nu}\frac{D}{k} = 1$$

$$\frac{D}{Nu}\frac{\partial Nu}{\partial D} = \frac{D}{Nu}\frac{h}{k} = 1$$

$$\frac{k}{Nu}\frac{\partial Nu}{\partial k} = \frac{k}{Nu}hD\left(-\frac{1}{k^2}\right) = -1$$

$$u_{Nu} = \pm\left\{\left[(1).\pm u_h\right]^2 + \left[(1).\pm u_D\right]^2 + \left[(-1).\pm u_k\right]^2\right\}^{1/2}$$

Here, $\dot{\forall}$ is volume flow rate, D is nozzle diameter, ν is kinematic viscosity and k is thermal conductivity of fluid. h, deals for convective heat transfer coefficient and is a function of Q (heat applied to the test section), A (heated area) and ΔT (temperature difference between coolant fluid and heated plate). Since h is not a dependent variable, it is necessary to calculate the uncertainty of this value with respect to the independent variables mentioned above, for the purpose of obtaining the uncertainty of Nusselt number.

Uncertainty calculation of h is given as an example below. It is obvious that the same procedure should be applied for obtaining the uncertainties of other parameters:

$$h = \frac{Q}{A\Delta T} = \frac{Q}{L^2\Delta T}$$

$$u_Q = \pm\frac{10W}{1000W} = \pm 0.01$$

$$u_A = \pm \frac{(1mm)^2}{(200mm)^2} = \pm 2.5 \times 10^{-5}$$

$$u_{\Delta T} = \pm \frac{0.1^\circ C}{7.86^\circ C} = \pm 0.127$$

$$u_h = \pm \left[\left(\frac{Q}{h} \frac{\partial h}{\partial Q} u_Q \right)^2 + \left(\frac{A}{h} \frac{\partial h}{\partial A} u_A \right)^2 + \left(\frac{\Delta T}{h} \frac{\partial h}{\partial \Delta T} u_{\Delta T} \right)^2 \right]^{1/2}$$

$$\frac{Q}{h} \frac{\partial h}{\partial Q} = \frac{Q}{h} \frac{1}{A \Delta T} = 1$$

$$\frac{A}{h} \frac{\partial h}{\partial A} = \frac{A}{h} \frac{Q}{\Delta T} \left(-\frac{1}{A^2} \right) = -1$$

$$\frac{\Delta T}{h} \frac{\partial h}{\partial \Delta T} = \frac{\Delta T}{h} \frac{Q}{A} \left(-\frac{1}{\Delta T^2} \right) = -1$$

$$u_h = \pm \left\{ \left[(1). \pm (0.01) \right]^2 + \left[(-1). \pm (2.5 \times 10^{-5}) \right]^2 + \left[(-1). \pm (0.012) \right]^2 \right\}$$

$$u_h = \pm 0.0162$$

Results of uncertainty analysis of the primary measurements are presented in Table 4.1 and 4.2. Table 4.1 includes the experimental uncertainties in measured quantities, and the Table 4.2 presents the calculated ones:

Table 4.1. Experimental uncertainties in measured quantities

Quantity	**Accuracy**	**Relative uncertainty**
$\forall$, volume = 0.55 ℓ	0.005 ℓ	u ($\forall$) = ± 0.009
t, time = 15 s	0.5 s	u (t) = ± 0.033
D, diameter = 5 mm	0.05 mm	u (D) = ± 0.01
Q, heat applied = 1000 W	10 W	u (Q) = ± 0.01
A, area = 40000 mm^2	1 mm^2	u (A) = ± 0.000025
Δ T, temperature diff. = 7.86ºC	0.1ºC	u (Δ T) = ± 0.0127

Table 4.2. Experimental uncertainties in calculated quantities

Quantity	Total relative uncertainty
$\dot{\forall}$, volumetric flow rate (ℓ/min)	$u\ (\dot{\forall}) = \pm 0.0345$
v, kinematic viscosity (kg/ms)	$u\ (\nu) = \pm 0.00197$
k, heat conduction coefficient (W/mK)	$u\ (k) = \pm 0.0002$
h, heat convection coefficient(W/m^{2}K)	$u\ (h) = \pm 0.0162$
Re, Reynolds number	$\boldsymbol{u}$ **(Re) = ± 0.036**
Nu, Nusselt number	$\boldsymbol{u}$ **(Nu) = ± 0.019**

4.2. Flow Visualization and Heat Transfer Coefficient Measurements

As it was mentioned in Chapter 3, the jet center plane is illuminated by a laser sheet and the images of the marker dye are acquired by a camera. During the experiments, the CCD camera is turned on as soon as the dye is injected. Experiments are ended when the dye clouded the test section such that it becomes impossible to distinguish the turbulent structures anymore. Usually some of the first and the last images are in poor quality due to either weak dye concentration or too much clouding and therefore those were deleted. Instantaneous images help us to understanding unsteady flow physics. On the other hand, a computer program that calculates the ensemble average of captured images is also developed by us, in order to see any overall characteristics of the flow for a given time period.

Actuation amplitude (1.5V and 2V of function generator outputs were fed to the amplifier), acoustic waveform (sine and square waves), nozzle-to-plate spacing "Z/D" (2, 4 and 6), nozzle geometry (sudden contracting, smooth contracting) and Strouhal number ($0 < St < 1$) effects are investigated.

It should be noticed that Reynolds number is kept near 10000 for all experiments. Uncertainty bars are not plotted in graphs, since it makes it hard to understand visually. Another important point is that, the lines linking the data points in the graphs are imaginary and have no physical meaning. Reported data are discrete and linking lines are just for the purpose of helping the reader to understand the possible trends in the data.

4.2.1. Effect of Acoustic Waveform

Ensemble averaged images of impinging jet with a smooth and sudden contracting nozzle are tabulated in Figure 4.1, 4.2 and 4.3. Nozzle-to-plate spacing, Z/D, is adjusted as 6 for Figure 4.1 and 4.2, where it is set as 4 for Figure 4.3. Flow is actuated with the sine and square waves. One fact which can be implied from Figure 4.1, 4.2 and 4.3 is the nearly same effect of sine and square waves on the shear layer of the jet flow. In accordance with this finding, whole discussions below are built on data with only sine waveform. Also, smooth contracting nozzle is tested with sine and square waveforms for Z/D=2, as it is seen from Figure 4.4, jet flow keeps on being laminar and acoustic actuation is seen to be ineffective. Some sample images are given for the case Z/D=2 in order to understand this situation.

4.2.2. Effect of Actuation Amplitude

Impinging jet with a sudden contracting nozzle is actuated with 1.5 and 2 Volts for two different Strouhal numbers. Depending on Figure 4.5 which illustrates heat transfer coefficient change with respect to Strouhal number, it can be suggested that actuation amplitude has such a low effect on heat transfer, and flow structures as it does not exceed the uncertainty limits. Similarly, flow visualization data for different nozzle types tabulated in Figure 4.6 leads us to the same idea. In accordance with this consideration, whole discussions below are built on data with 2 Volts amplitude.

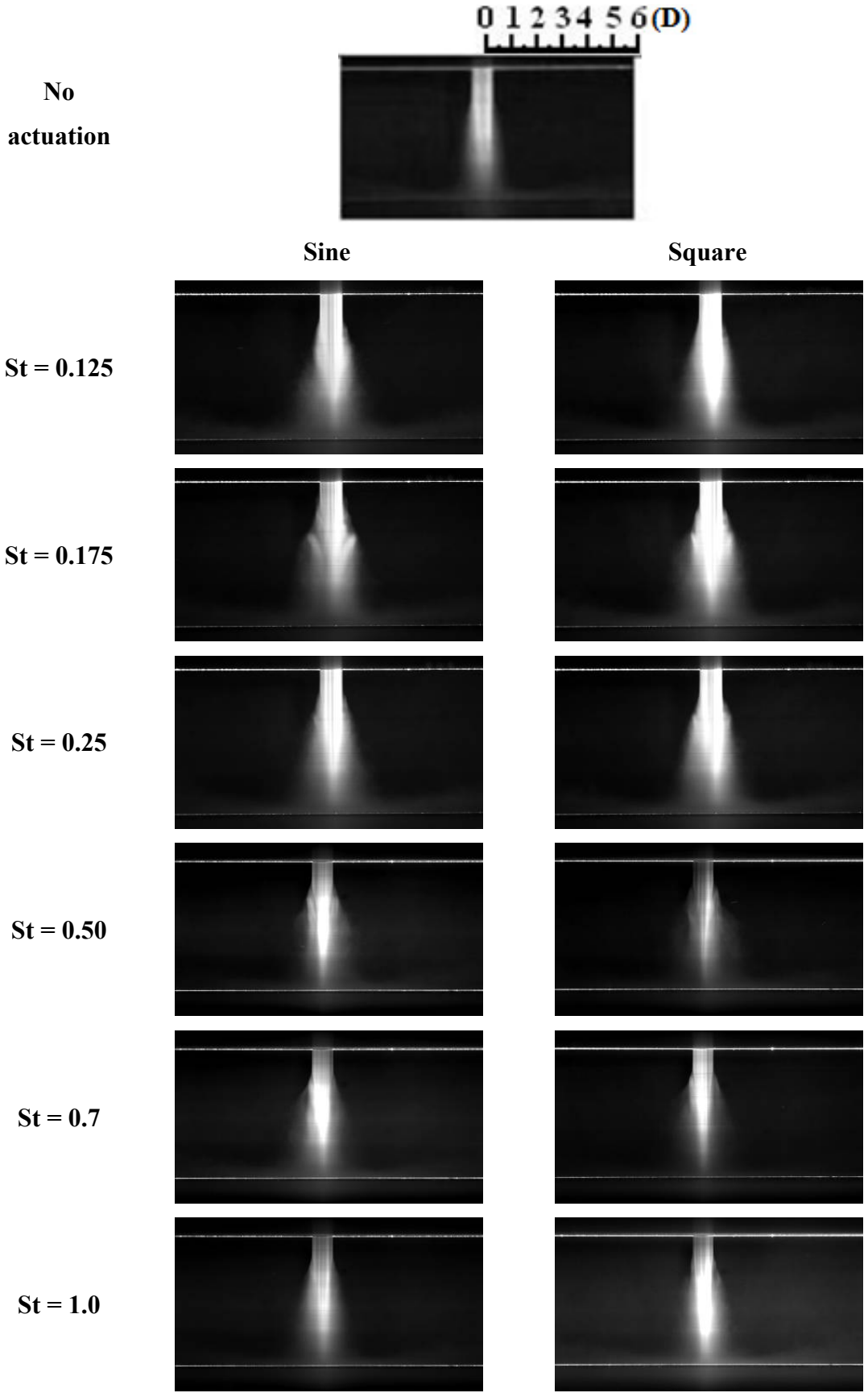

Figure 4.1. Ensemble averaged images, Smooth CN, Z/D=6, Amplitude=2V

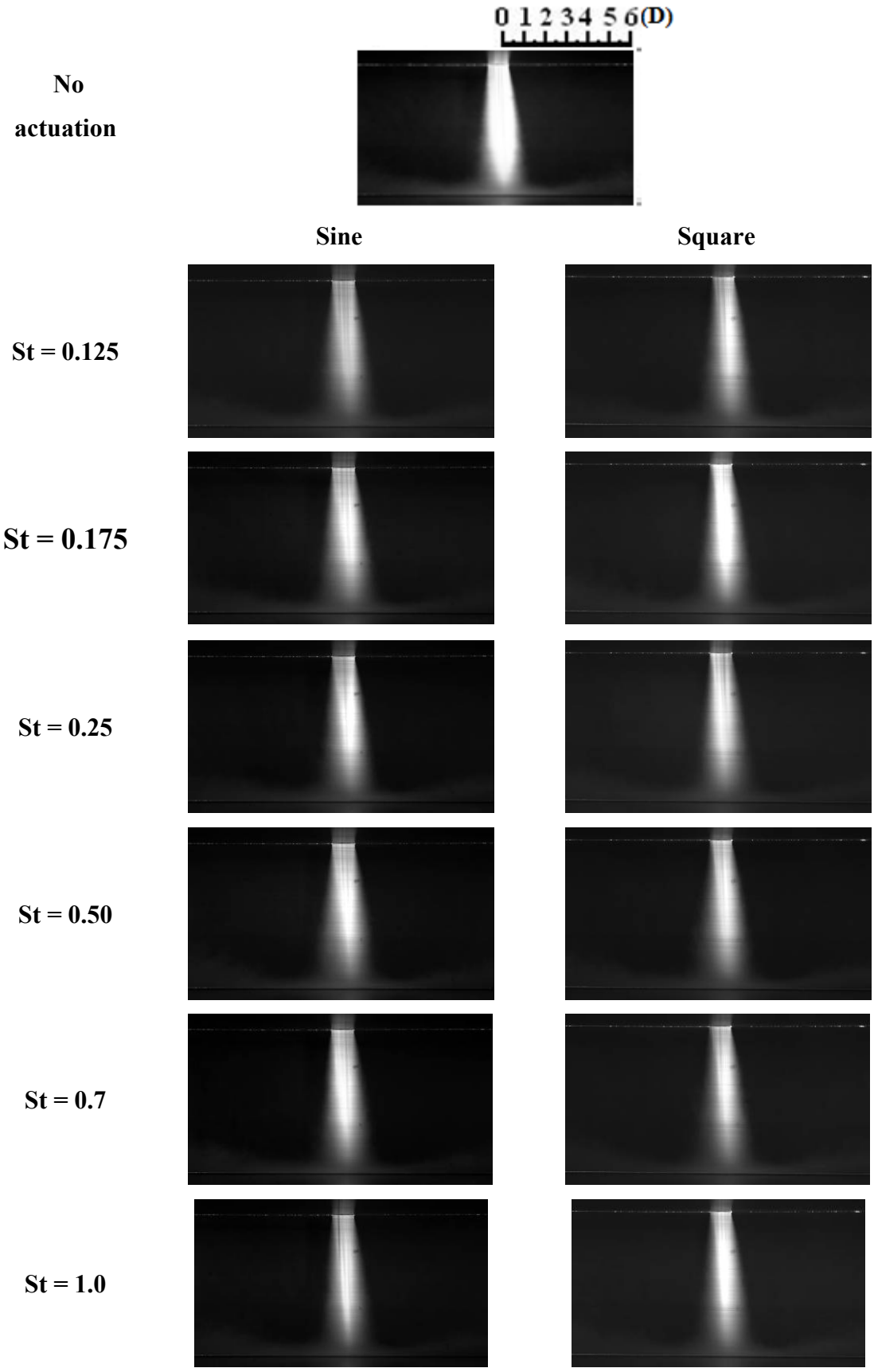

Figure 4.2. Ensemble averaged images, Sudden CN, Z/D=6, Amplitude=2V

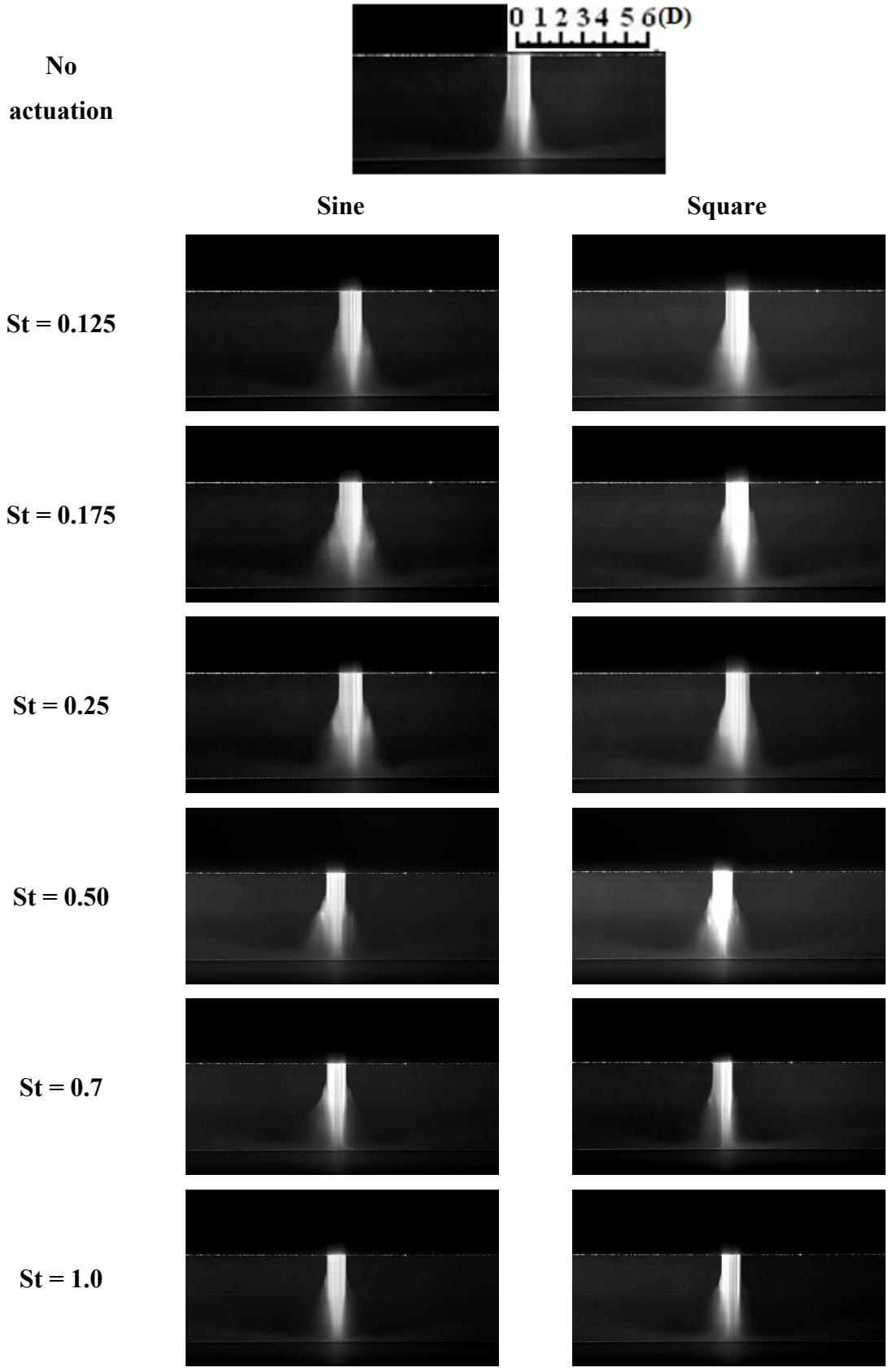

Figure 4.3. Ensemble averaged images, Smooth CN, Z/D=4, Amplitude=2V

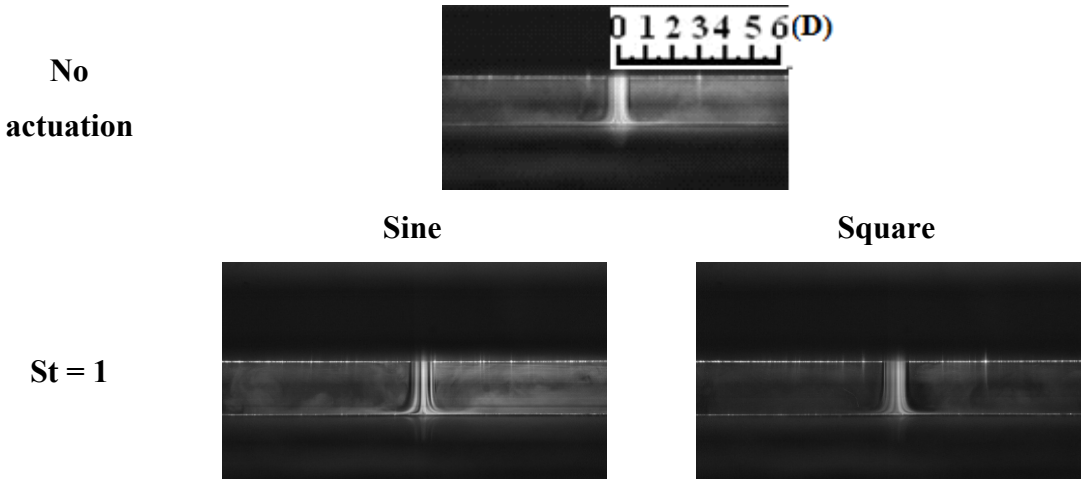

Figure. 4.4. Instantaneous images, Z/D=2, Sine, Amplitude=2V

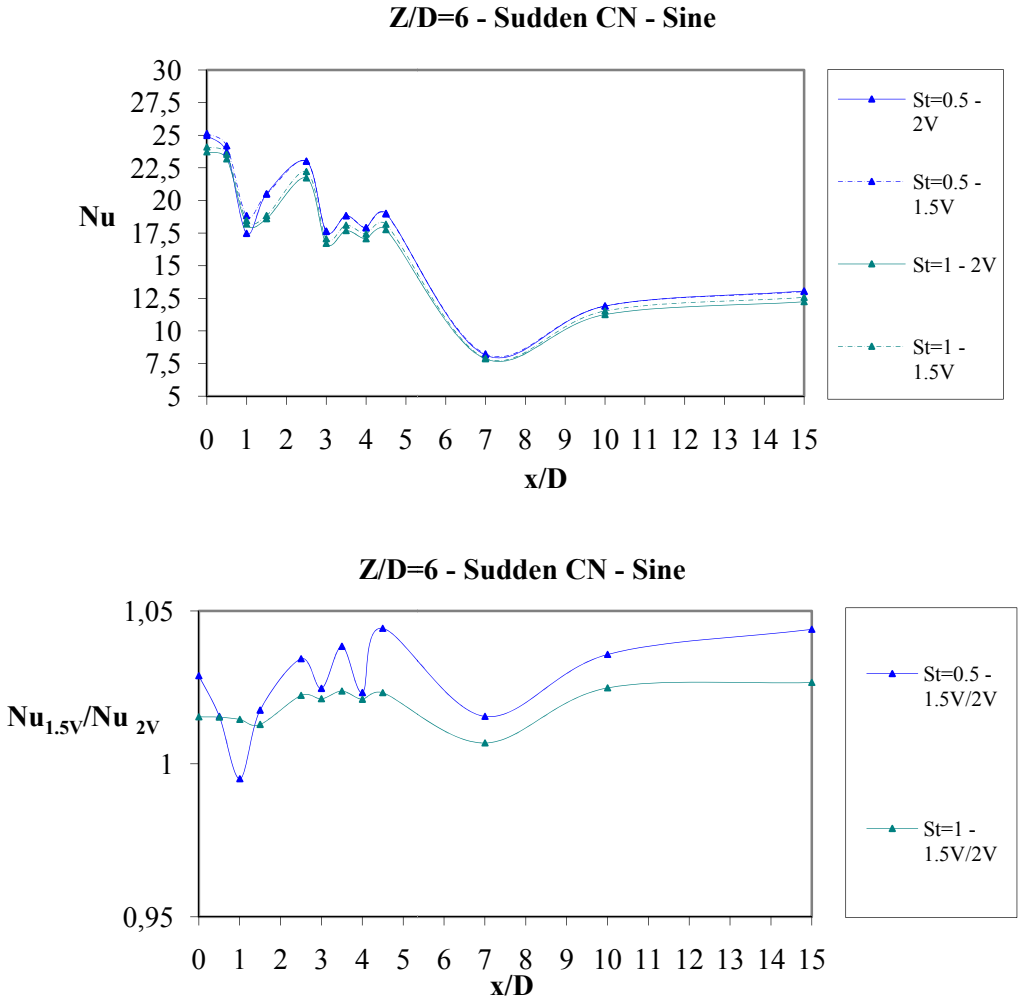

Figure 4.5. Effect of actuation amplitude. (1.5V case normalized with 2V case)

4.2.3. Effect of Nozzle-to-plate Spacing and Strouhal Number

Strouhal number (St) has a spreading effect on jet flow. For St=0.175, a sharp and a steady roll-up effect is seen at z/D=2, as this effect leads to a spreading on the jet shear layer. The roll-up structures can be seen in Figure 4.6. Thus, it can be said that this steady roll-up occurs continuously during the actuation and it is significant for only smooth contracting nozzle.

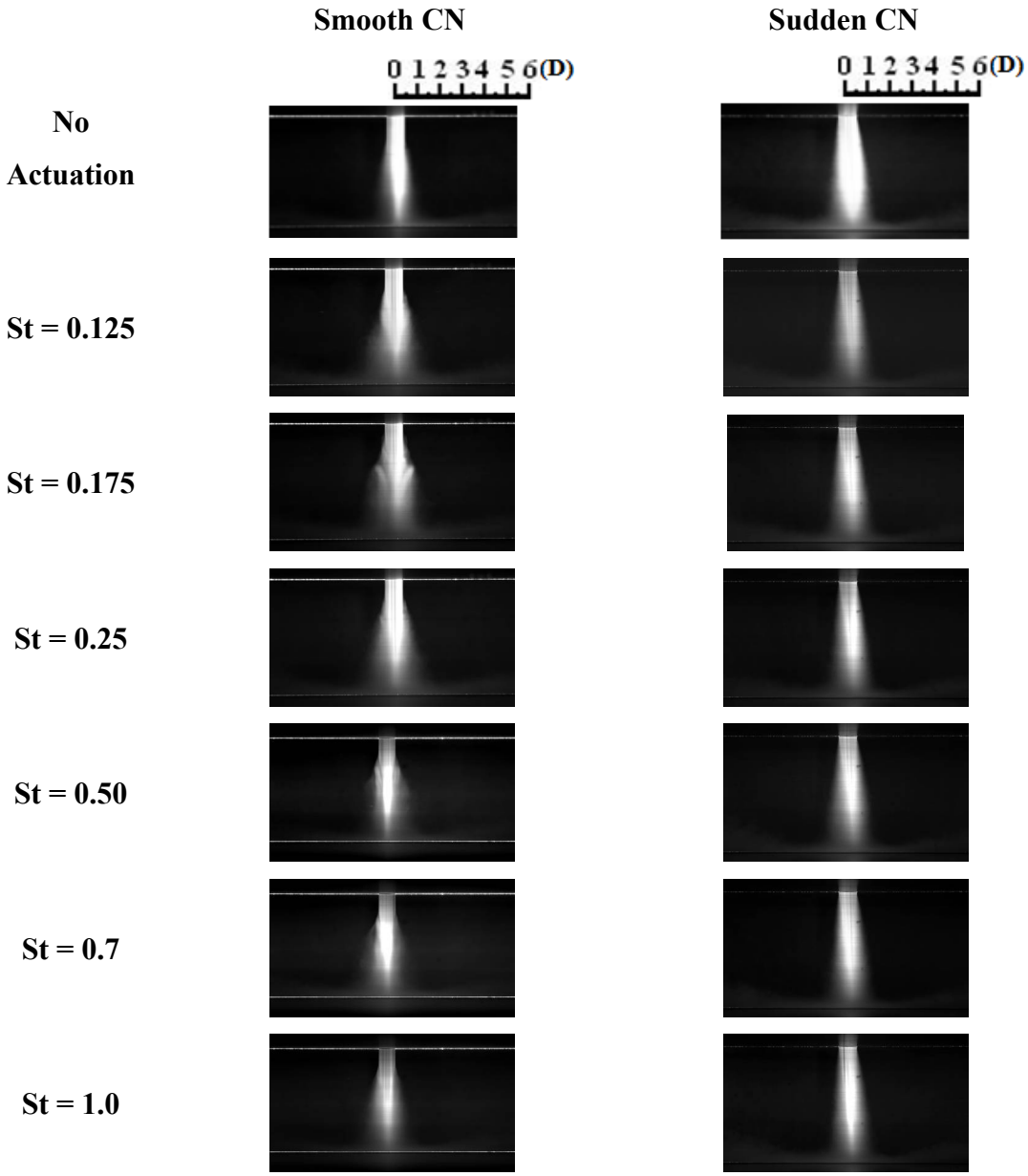

Figure. 4.6. Ensemble averaged images, Z/D=6

Roll-up can be seen more clearly in an instantaneous image such as those tabulated in Figure 4.7 and 4.8. It should be noted that, while Figure 4.7 includes the data for St=0.175 where most outstanding occurrence of roll-up structures is seen. Figure 4.8 includes a variety of different actuation cases. Images tabulated in the latter are captured by means of a high speed camera, so that structures can be seen in detail perfectly.

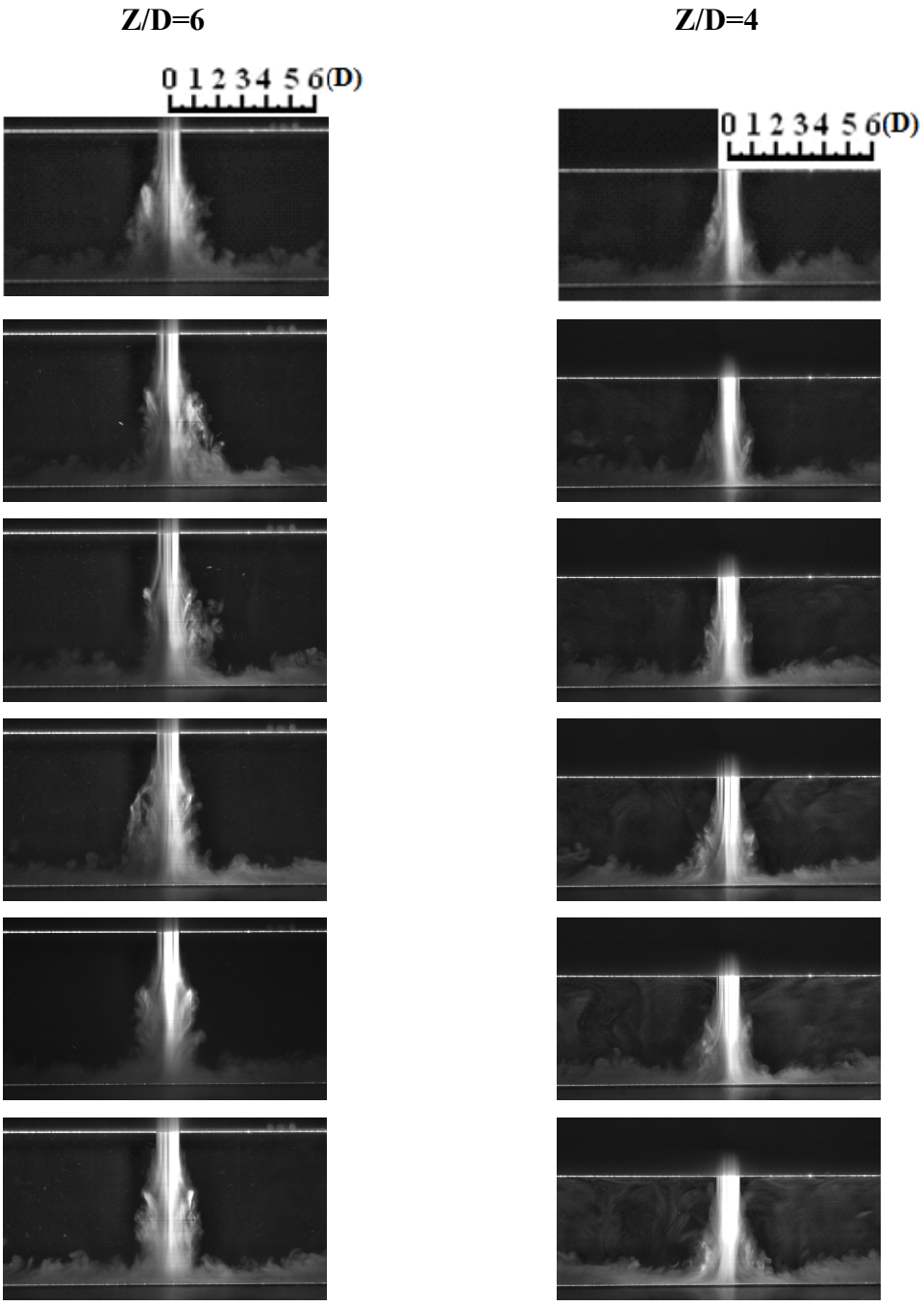

Figure. 4.7. Instantaneous images, Smooth CN, St=0.175

From Figure 4.7, it can be obviously seen that, roll-up structure occurs at an axial distance of about z/D=2. Images clearly show that roll-up structure is axi-symmetric for all cases. For the case Z/D=6, roll-up structure is so strong that the jet gets narrower after the roll-up. At Z/D=4 configuration, this roll-up process occurs as well, but because of the short distance between the stagnation point and the roll-up occurrence position, the flow and roll-up structure itself deeply interact with this high pressurized zone and it becomes impossible for the roll-up structure to evolve into a coherent structure. The coherent and incoherent structures formed by this roll-up process are worth studying in a fluid-mechanical approach; nevertheless, they have no significant effect on heat transfer, as it will be seen in following sections.

Roll-up effect loses its sharpness when St=0.25. Another roll-up effect which is not as significant as in St=0.175 is seen at St=0.5. For Strouhal numbers between 0.5 and 1, roll-up starts to diminish and it loses its character as St=1. An interesting point is that for St=1, spreading of the jet is similar to the one for no actuation case.

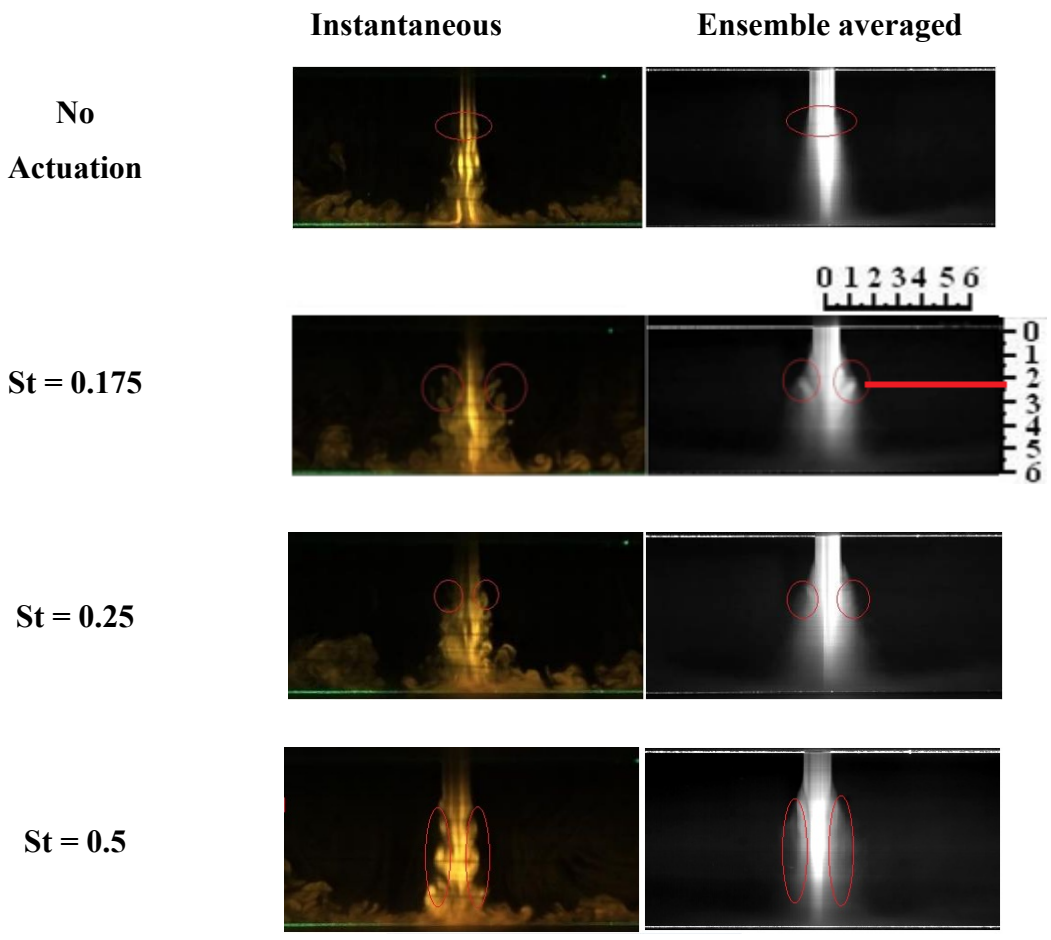

Figure. 4.8. Instantaneous vs ensemble averaged images, Smooth CN, Z/D=6

The changes in the jet shear layer plays a little but nearly insignificant role on heat transfer. Figure 4.9 illustrates the effects of Strouhal number on heated plate Nusselt number at different nozzle-to-plate spacing ratios, for the smooth contracting nozzle which is actuated with a sine wave. Actuated cases for each nozzle-to-plate spacing values are normalized with no actuation case. The most striking feature seen from these figures is that the effect of the acoustic actuation is most dominant in the stagnation region. The difference between the Nusselt numbers diminishes with increasing radial distance x/D. There is almost no difference in Nusselt numbers beyond x/D=5. Which is to say that our acoustic perturbation has no effect beyond x/D=5. Moreover, Nusselt number takes its smallest value for the lowest Strouhal number for each Z/D case. Nu numbers also increases with the increasing Strouhal number. No acoustic actuation gives the highest Nusselt number for Z/D=6. As for the Z/D=4 and 2, although it is still high, its corresponding Nusselt number is slightly lower than the St=1 case. It's also seen from the figures that, increasing Z/D has slightly increased the heat transfer coefficient.

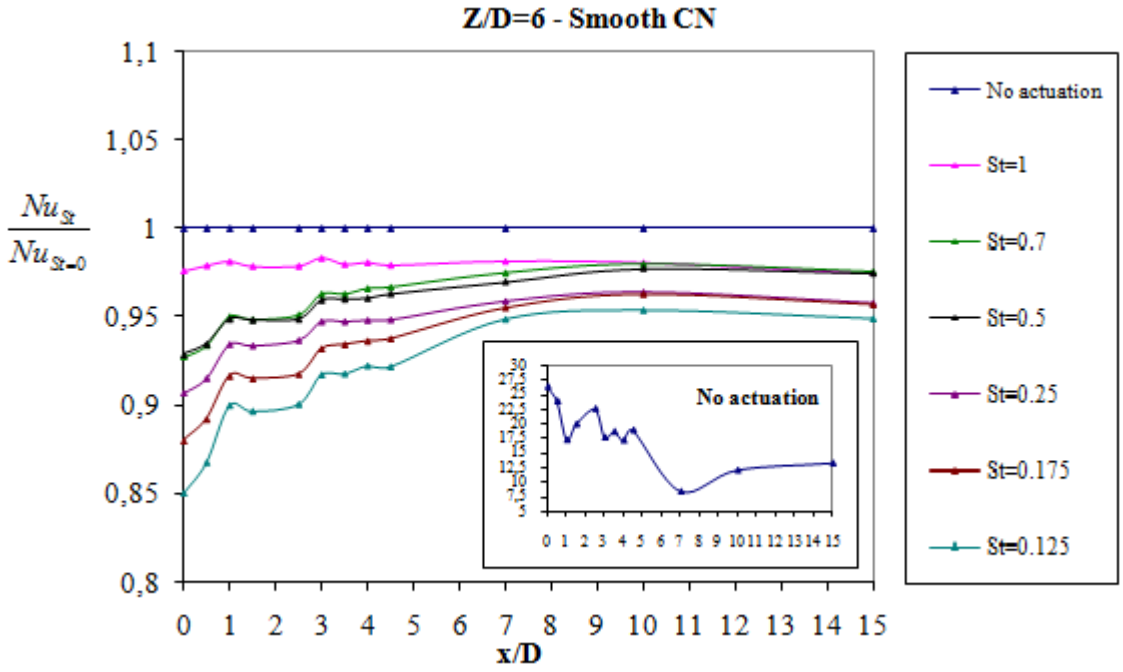

Figure. 4.9. Nusselt number distribution on the hot plate, Smooth CN (normalized with stagnation point Nu number)

(cont. on next page)

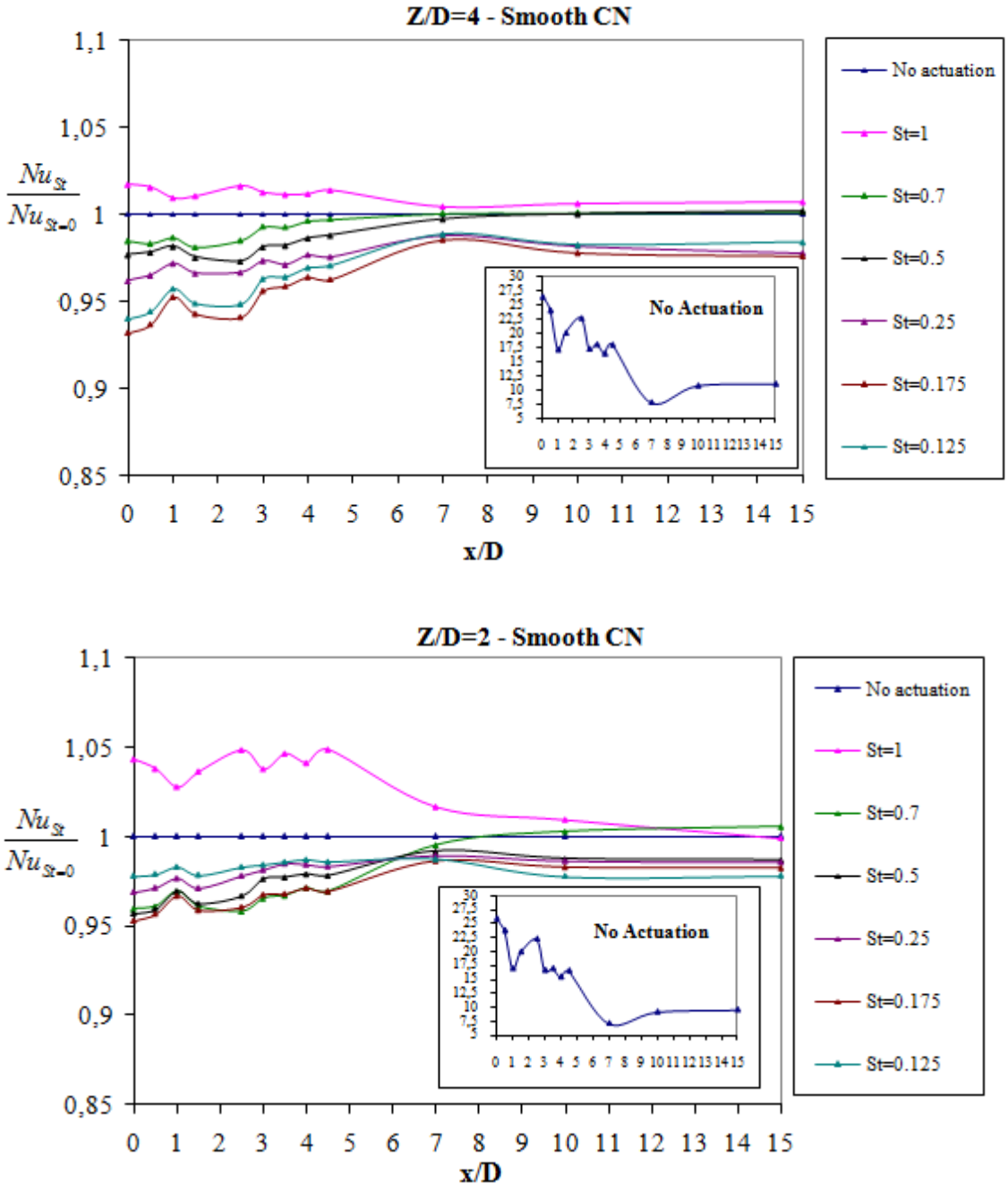

Figure. 4.9. (cont.)

The distribution of Nu number shows that, beyond the maximum at the stagnation point, heat transfer coefficient decreases in the radial direction up to x/D=1. This minimum is followed by another peak at x/D=2.5, and then another decrease. Nusselt number makes a plateau between 3 < x/D < 4.5. Beyond the x/D=4.5, Nusselt number decreases upto x/D=7 and with a slight increase plateaus beyond that.

These Nusselt number profiles also suggest that the seemingly laminar flow for Z/D=2 (Figure 4.4) also has the almost the same heat transfer characteristics. This can

be explained by the fact that the flow regime of the wall-jet is a turbulent one even though the jet itself is a laminar one.

4.2.4. Effect of Nozzle Geometry

Two different types of nozzles are used in the scope of this thesis, as it was mentioned in Chapter 3:

- Smooth contracting nozzle in the form of a fifth degree polynomial (See Figure 3.3-b),
- Sudden contracting nozzle.

As it can be seen from Figures 4.1, 4.2 and 4.3, the shear layer of the jet flow with a smooth contracting nozzle becomes turbulent at about $z/D \approx 1$. On the contrary, the shear layer originated from the sudden contraction becomes turbulent as soon as it comes out. The reason of this behaviour is thought to be the turbulence decaying effect of smooth contracting nozzle. Moreover, most probably flow separates in the entrance of the sudden contraction and is turbulent entirely in it. Since the turbulence intensity is high for sudden contracting nozzle with respect to smooth contracting one, transition to turbulence occurs suddenly. Furthermore, the roll-up structures observed in smooth contracting nozzle at $St=0.175$, are not seen in the sudden contracting nozzle due to most probably high turbulence levels. Effects of different nozzle geometries on Nusselt number are plotted on Figure 4.10. Also, instantaneous images of jet flow for nozzle-to-plate spacing $Z/D=6$ are given in Figure 4.11 for the purpose of comparing the nozzle geometry effect.

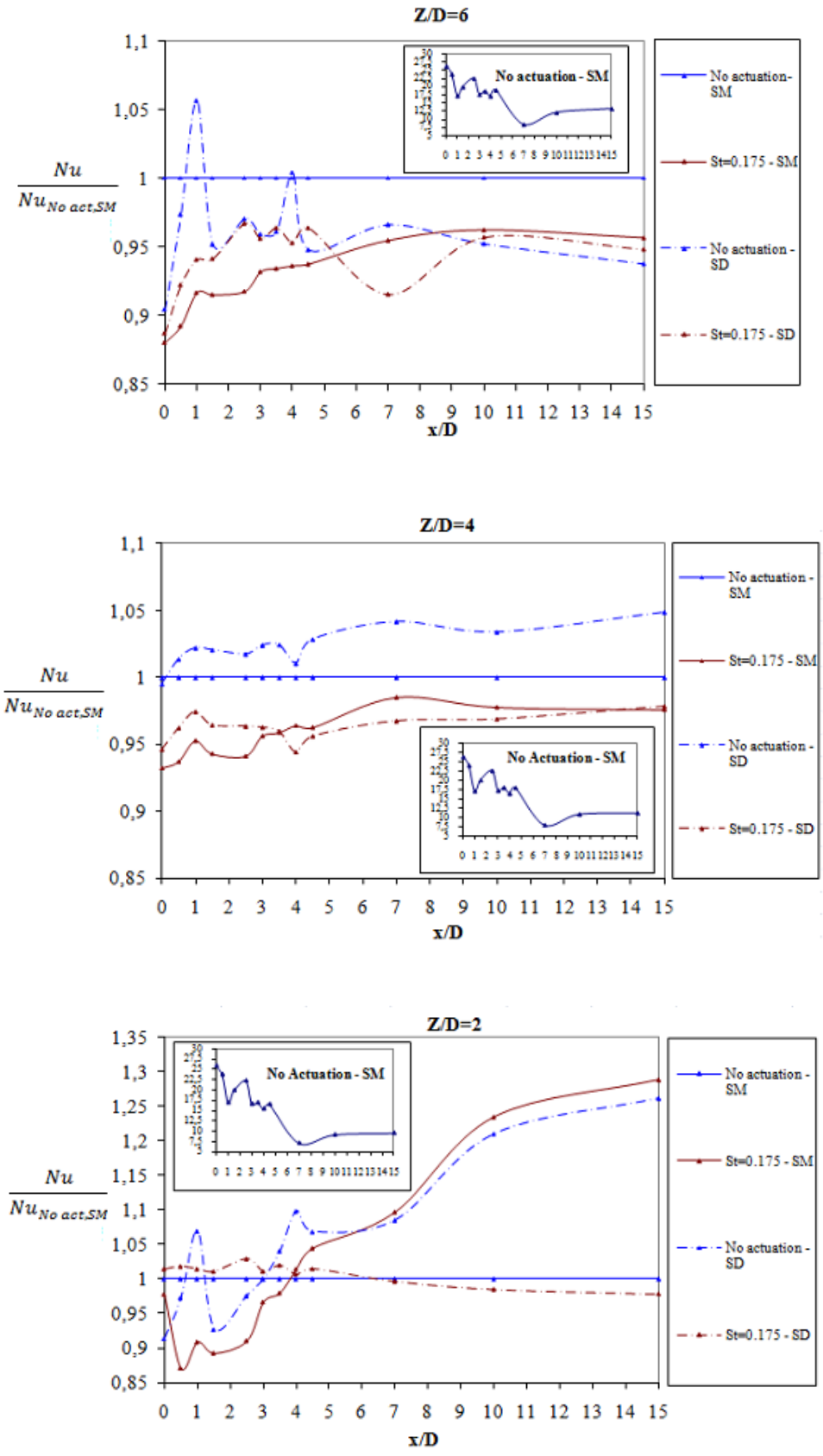

Figure. 4.10. Nusselt number distribution on the hot plate, various nozzle geometries (Normalized with No actuation, Smooth CN case)

In accordance with the similar form of Nusselt number curves for different cases, it can be suggested that these profiles are almost independent from nozzle geometry especially at small x/D's. This finding leads us to suggest the independent growth of wall-jet shear layer from the nozzle geometry. The distribution of Nu number with respect to axial distance x/D for different cases show us again that, maximum (x/D=0, 2.5, 3.5, 4.5) and minimum (x/D=1, 3, 4, 7) peaks occurs at the same locations, consistently. Besides, of course, some differences are observed and their possible reasons are discussed below.

Investigating the Figure 4.10 in close detail shows that smooth contracting nozzle provides a higher heat transfer coefficient in the stagnation region in comparison with sudden contracting nozzle, for Z/D=6. This situation is also recognized in wall jet region, for no actuation case. On the other hand, for St=0.175 case, it is observed that sudden contracting nozzle result in clearly higher heat transfer coefficients at the stagnation region, however, in outer boundaries of the wall jet, smooth contracting nozzle gives higher heat transfer.

For Z/D=4, the sudden contracting nozzle results in higher heat transfer coefficient at any region when there is no actuation. As the jet is actuated with St=0.175, the same behaviour of the actuated jet for Z/D=6 is seen: Sudden contracting nozzle results in higher heat transfer coefficients at the stagnation region, but smaller heat transfer coefficients at outer boundaries.

The data for Z/D=2 is more complicated and hard to comment about. However, it can be clearly recognized that, for the radial distance of x/D>5, smooth contracting nozzle provides a significant enhancement in heat transfer for no actuation case. On the other hand, for St=0.175, sudden contracting nozzle shows a nearly same performance.

Though the absence of data about turbulence makes it harder to comment about those phenomenons, the dissimilarities of wall-jet shear layers are thought to be the reason of all mentioned above. The effect of different nozzle geometries can be considered as a result of their differentiating initial turbulence intensities. Velocity measurements with hot-wire anemometers – which is out of the scope of this work - in the vicinity of jet inlet and wall-jet regions must be performed to get a better understanding on this mechanism in a fluid mechanical approach. This evidence is also pointed out in literature by Jambunathan et al. (1993)

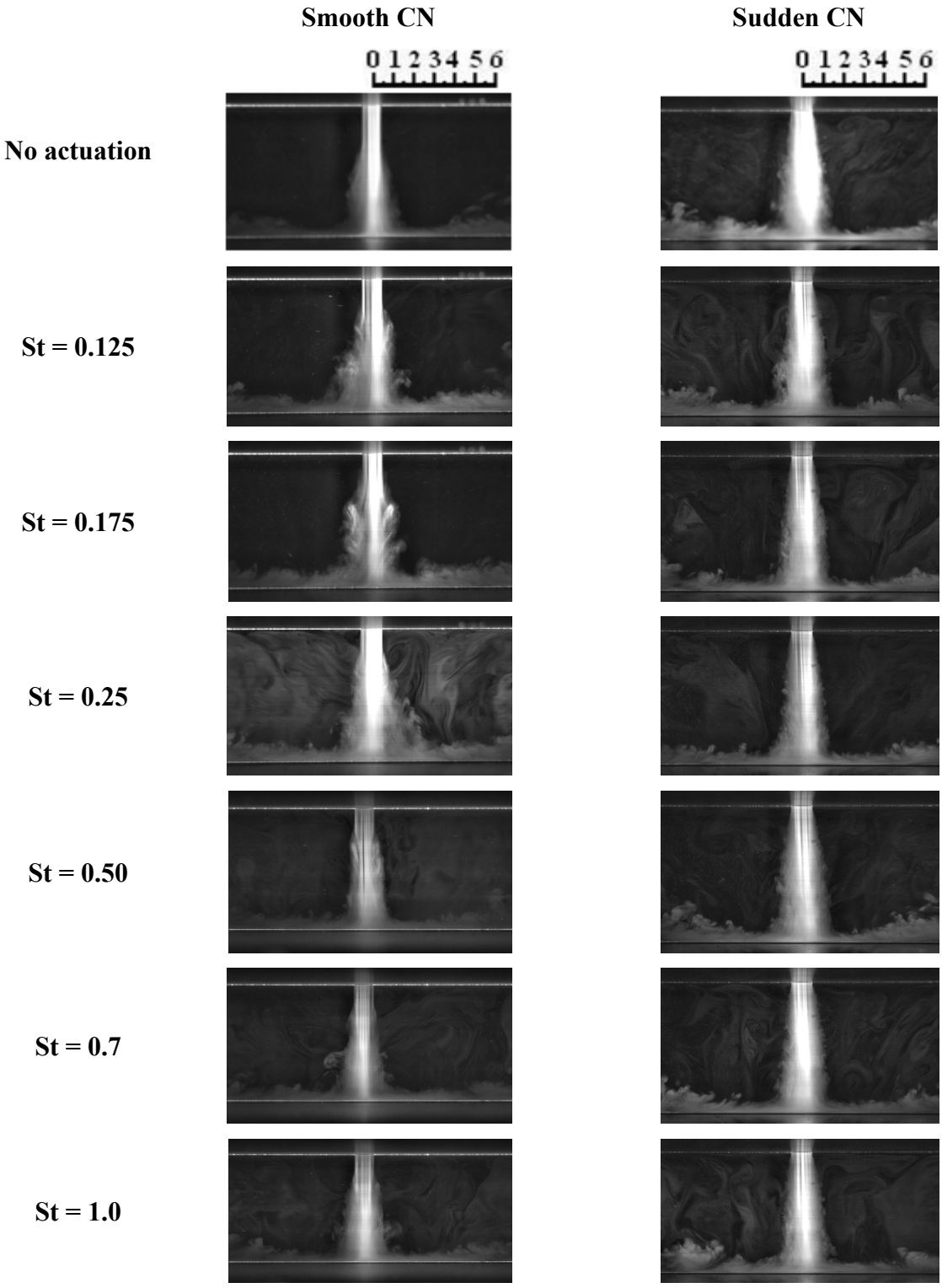

Figure 4.11. Instantaneous images, Z/D=6, Amplitude=2V

Figure 4.11 also sheds light on the fact that, flow structures of the impinging jet with a sudden contracting nozzle are not affected from the actuation. In contrast with the smooth contracting nozzle, the jet does not spread and seems to be unaffected from

any frequency of acoustic waves. It is thought that, acoustic actuation of $0 < St < 1$ cannot alter the flows' natural instabilities, since the flows intense turbulence takes over our small perturbation. Moreover, the sudden contracting nozzle itself is considered to be as a source of instabilities. This phenomenon is also suggested in literature (Mankbadi et al. 1989) as it was mentioned in Chapter 2.

4.2.5. Effect of St Number on Stagnation Point Nu Number

Figure 4.12, which shows the effect of the actuation frequency on stagnation point Nusselt number, addresses two important facts: First, the waveform of the actuation (either if it is sine, nor square wave) does not have an important role on Nu number. The differences between graphs are not that significant, whereas those differences can be interpreted in the uncertainty limits of our experiments. Second, a decrease in nozzle-to-plate spacing from Z/D=6 to 4 leads an increase in Nusselt number for all Strouhal numbers.

As for the Z/D=2, the profile of Nu number gets changed, but its magnitude stays almost-constant. It can be suggested that, shear layers in the stagnation point are almost same for Z/D=2 and 4, and are nearly laminar, whereas for Z/D=6, shear layer shows a different characteristic in some way.

Nozzle geometry with a smooth contraction causes stagnation point Nu number change less slowly with St number. Again, jet with a nozzle-to-plate spacing ratio of Z/D=6 gives the lowest Nu number. For the cases Z/D=2 and 4, though the Nu number distributions are nearly same for $0 < St < 0.25$, as for up to St=0.6, Nu number patterns a diminishing character. Nevertheless, for St=1, Nu number reaches to the same level for both cases.

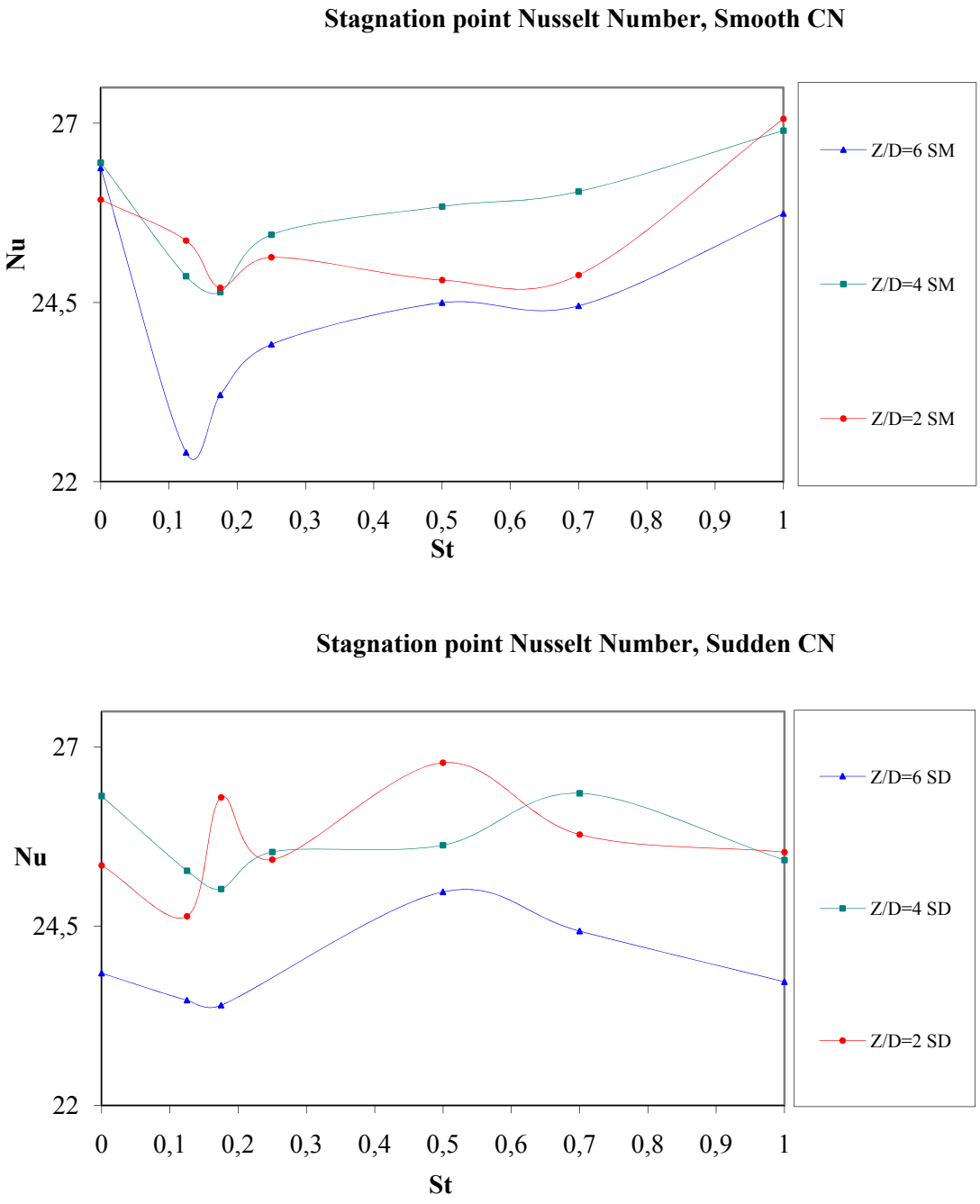

Figure. 4.12. Stagnation point Nu number for various St numbers, Sudden CN

Another point, which is seen in Figure 4.12 is that there is an consistent minimum for $0.1 < St < 0.2$ for all cases. It is considered that, the spreading effect of the acoustic vibrations which causes a decrease in the centreline velocity on stagnation point causes a thickening effect on wall jet layer. This evidence leads to a decrease in Nusselt number. As the Strouhal number gets bigger, small scale eddies arise, hence they cause an additional mixing effect and let Nusselt number get higher.

4.2.6. Average Surface Nusselt Number

Although the surface average Nu number distribution of heated plate with respect to Strouhal number which are graphed in Figure 4.13 look very complicated, there are some significant points that should be noted. There is a consistent minimum for the range of $0.1 < St < 0.2$. As it was mentioned in Figure 4.12, a minimum for St=0.1 for stagnation point Nu number is consistently seen. This fact leads us to the idea that the case St=0.1 causes a decrease in heat transfer not only in stagnation point, but also in whole heated plate.

One other thing we can see is the different behaviour of the case Z/D=2 with smooth contracting nozzle with an exception that it makes a minimum at St=0.175. In contrast with the rising characteristic of Nu number for $0.2 < St < 1$ for all other cases, any increase is not seen for Z/D=2 with smooth contracting nozzle until St=0.7, but then a sudden increase is noted up to St=1.

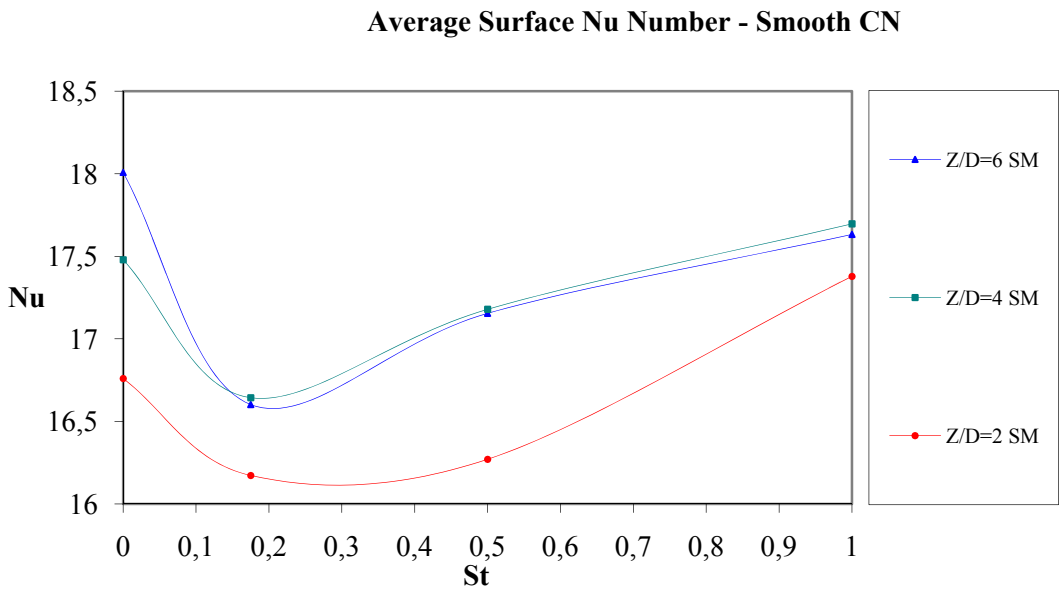

Figure. 4.13. Average Surface Nu numbers for various Z/D

(cont. on next page)

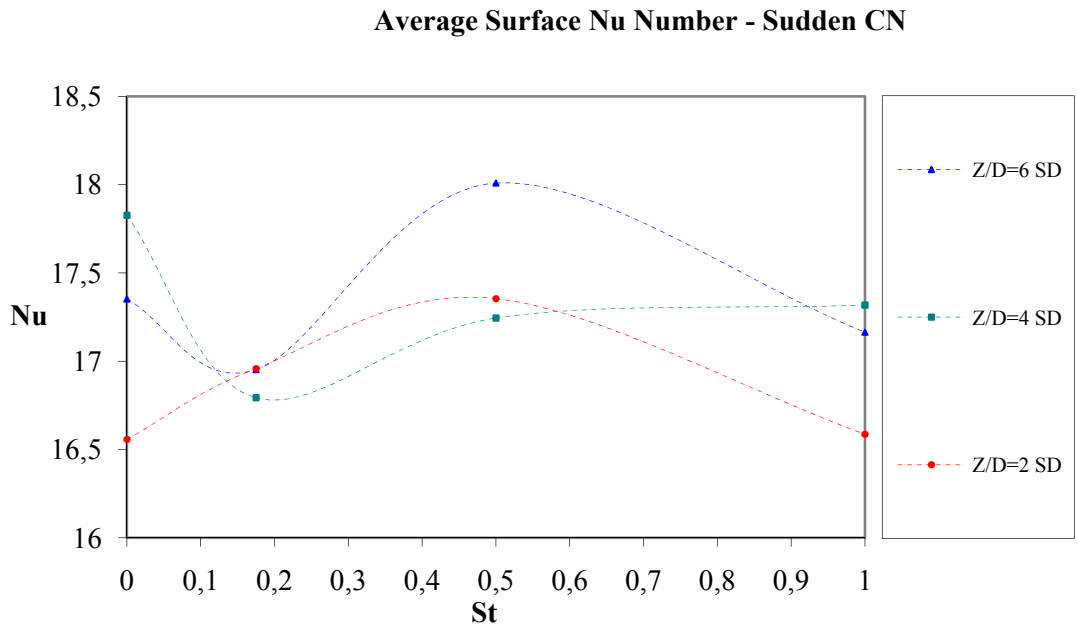

Figure. 4.13. (cont.)

4.2.7. Reproducibility of Experiments

For the purpose of testing the reproducibility of our experiments, some experiments are repeated by different people on different days. The results are illustrated in Figure 4.14, where the results discussed above are normalized with reproducibility experiments' results. It is obvious that, our experimental results are consistent and they are nearly between the borders of our uncertainty limits.

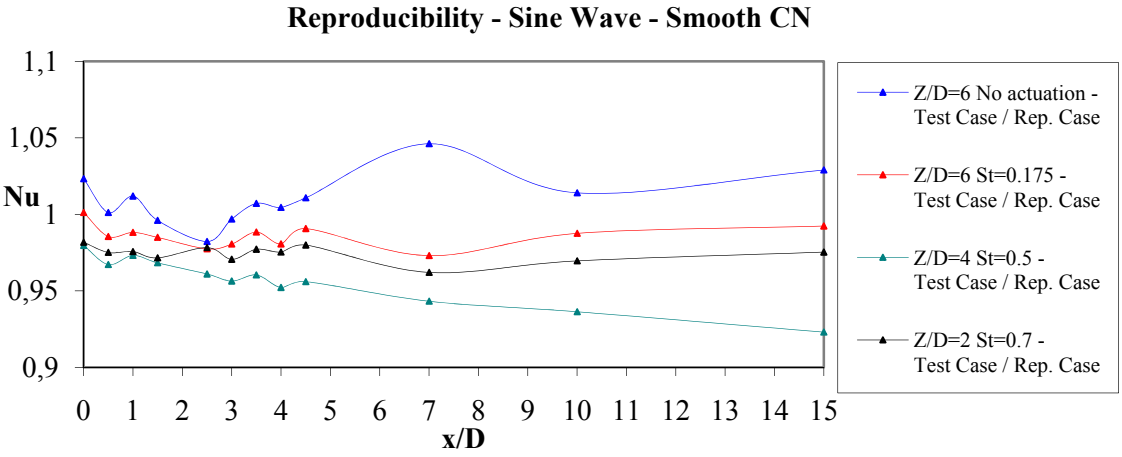

Figure. 4.14. Reproducibility of experiments

4.2.8. Comparison with Other Studies and Correlations

Experimental results of this study are compared with other studies mentioned in the literature survey. Also, the correlation offered by Martin (1986) – *see equation (2.1)* – is used for comparison (Note that Martin's equation is valid for $1.5 \leq x/D \leq 7.5$ and $2 \leq Z/D \leq 12$). In Figure 4.15, Nusselt number distributions of different researchers are given, where Nusselt number at any point is normalized with stagnation point Nusselt number. Though the boundary conditions of the studies are different from each other, it can be said that our experimental results are clearly in the order of the results which are reported in the literature.

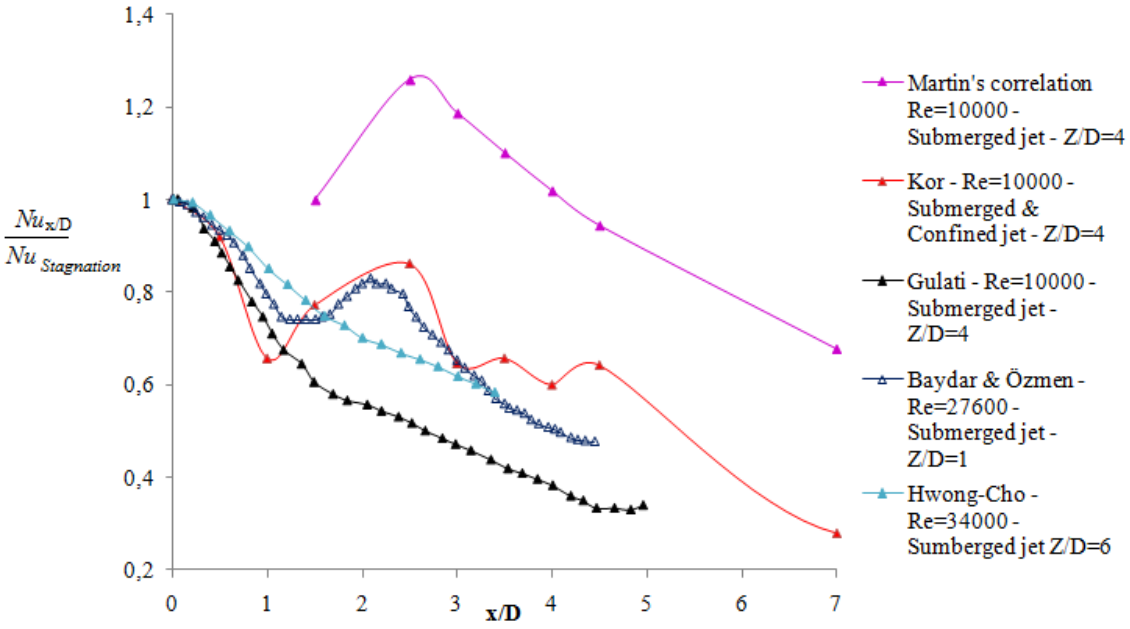

Figure. 4.15. Comparison with other studies

CHAPTER 5

CONCLUSIONS

Flow visualization and heat transfer experiments of an acoustically actuated round jet which is a combination of submerged and confined jets are performed in the scope of this work, with the purpose of having a better understanding on acoustic actuation's effect on heat transfer performance. Reynolds number is kept at around 10000 for all experiments. Dimensionless nozzle-to-plate spacing, Z/D, is adjusted as 2, 4 and 6. Non-dimensional expression of acoustic frequency, Strouhal number, is changed in the range of $0<St<1$. Actuation with sine and square waveform is applied with the amplitude of 1.5 and 2 Volts. Two nozzle geometries are used during experiments: smooth and sudden contracting nozzles.

It is understood from these experimental data that, both acoustic waveforms (sine and square) give nearly same results for heat transfer. Also, similar flow characteristics are observed for each case. Similarly, voltages sent to 20X amplifier, which are 1.5 and 2 Volts, give very close results.

Nozzle-to-plate spacing and actuation Strouhal number are found to be very effective especially on flow structures observed in smooth contracting nozzle. For nozzle-to-plate spacing of 6 nozzle diameters, with the actuation frequency of St=0.175, a sharp, continuous and significant roll-up evidence is seen at axial location of about z/D~2, which spreads the jet dramatically. Roll-up effect loses its sharpness when St=0.25. Another roll-up effect which is not as significant as St=0.175 seen again at St=0.5. For Strouhal numbers between 0.5 and 1, roll-up starts to diminish and it loses its character totally at St=1. A similar structure is obtained at the same location for Z/D=4, however, since the location it is formed is so close to the stagnation zone, it does not cause an additional spreading in the jet. This phenomenon in smooth contracting nozzle is seen in heat transfer. For Z/D=6, acoustic actuation has caused a decrease in heat transfer. In contrast, for nozzle-to-plate spacings 2 and 4, acoustic frequency corresponding to St=1 resulted in an increase in heat transfer coefficient.

Transition to turbulence in the shear layer of the jet is obtained at $z/D\approx1$ for smooth contracting nozzle. Nevertheless, no laminar region is observed for sudden contracting nozzle, as the shear layer in this case became turbulent immediately.

Furthermore, acoustic actuation is found to be ineffective in sudden contraction, because of the flows' high intensity turbulence. Nevertheless, these differences in flow properties do not make significant effect on the Nusselt number distribution.

Z/D=4 is found to be more effective on stagnation point heat transfer with respect to Z/D=6, for all Strouhal numbers. As for the Z/D=2, the profile of stagnation point Nu number gets changed, but its magnitude stays almost-constant, as compared with Z/D=4. Moreover, St=1 gives the same stagnation point Nusselt number for Z/D=2 and 4.

A minimum peak is seen for the range $0.1<St<0.2$ not only in stagnation point, but also surface average Nusselt numbers, which make us consider that this characteristic is not a local, but an overall property for any point on the heated plate.

It must be noted that, in contrast with the literature, the impinging jet region is confined not only by the walls at both sides, but also by the top plane. It is thought that, this situation has caused the coolant circulate in the jet room. Hence, while some of the coolant is moved away from the test section immediately, a considerable amount of it continued stay in jet room with the heat which it gained from the heated plate. This phenomenon is thought to be the reason of uncommon distribution of Nusselt number in our studies.

Some recommendations about the future works for this study may be presented as:

- The temperature of the circulating coolant in the jet room can be measured for a better understanding about the effect of confinement.
- Temperature distribution of the plate in various radial directions should be measured to understand if the temperature distribution is symmetric or not.
- Heat transfer in an in-line or confined jet should be investigated experimentally for comparing the results with respect to this thesis.
- Higher heat flux should be applied to the heated plate.
- Velocity fluctuations caused by turbulent structures obtained at certain Strouhal numbers should be measured by hot wire instruments.
- Statistical meaning of turbulence should be discussed, as it will give the researcher more understanding on turbulence characteristics.
- Since sudden contracting jet is thought to be more receptive to higher Strouhal numbers, flows' response to higher frequencies should be investigated.

- Turbulence intensity and velocity measurements should be performed for wide range of radial distance.
- Effects of initial turbulence intensity should be investigated on the Nusselt number, especially for the Strouhal numbers found to be effective in this thesis.
- Pressure measurements should be performed on the impinging plate and the jet inlet plane must be performed.
- Extensive velocity measurements ought to be done with optical methods such as Particle Image Velocimetry.
- Different actuation methods can be used in order to compare obtained results with respect to this study, such as fluidic actuators.
- Different nozzle geometries can be used for the purpose of comparing its result with respect to this study.

REFERENCES

Baydar, E., Ozmen, Y. 2005. An experimental and numerical investigation on a confined impinging air jet at high Reynolds numbers, Applied Thermal Engineering, Vol.25, pp.409-421

Baydar, E., Ozmen, Y. 2006. An experimental investigation on flow structures of confined and unconfined impinging air jets, Heat and Mass Transfer, Vol.42, pp.338-346

Bhattacharya, S., Ahmed, A. 2010, A note on unsteady impinging jet heat transfer, Experimental Thermal and Fluid Science, Vol. 34, pp.633-637

Bilgin, N., 2009, Experimental investigation of heat and fluid flow in an actuated impinging jet flow, M.Sc. Thesis, İzmir Institute of Technology

Celik, N., Eren, H. 2009. Heat transfer due to impinging co-axial jets and the jets' fluid flow characteristics, Experimental Thermal and Fluid Science, Vol.33, 715-727

Clifford, A. B. 2005. Acoustics of excited jets-A historical perspective. NASA/TM 2005-213889, Glenn Research Center, Cleveland, Ohio

Crow, S.C., Champagne, F. H. 1971. Orderly structure in jet turbulence. Journal of Fluid Mechanics, Vol. 48, pp.547-591

Den Ouden, C., Hoogendoorn, C. J. 1974. Local convective heat transfer coefficients for jets impinging on a plate: experiments using a liquid-crystal technique. Proc. 5th Int. Heat Transfer Conf., Japan, Vol. 5, pp. 293-297

Fox, R.W., McDonald, A.T., Pritchard, P.J., 2004, Introduction to fluid mechanics, 6th edition, John Wiley and Sons Inc., USA, pp. 755-761

Gardon, R., Akfırat, J. C. 1965. The role of turbulence in determining the heat transfer characteristics of impinging jets. Int. J. Heat and Mass Transfer, Vol.8, pp.1261-1272

Gardon, R., Carbonpue, J. 1962. Heat transfer between a flat plate and jets of air impinging on it. Int. Developments in Heat Transfer, Int. Heat Transfer Conference, USA, pp. 454-460

Gautner, J. W., Livingood, J. N. B. and Hrycak, P. 1970. Survey of literature on flow characteristics of a single turbulent jet impinging on a flat plate. NASA TN D-5652 NTIS N70-18963

Goldstein, R. J., Behbahani, A. I. and Kieger, H. K. 1986. Streanwise distribution of the recovery factor and the local heat transfer coefficient to an impinging circular air jet. Int. J. Heat Mass Transfer, Vol.29, pp.1227-1235

Gulati, P., Katti, V., Prabhu, S.V. 2009. Influence of the shape the nozzle on local heat transfer distribution between smooth flat surface and impinging air jet, Int. Journal of Thermal Sciences, Vol.48, pp.602-617

Gundappa, M., Hudson, J.F., Diller, T.E. 1989. Jet impingement heat transfer from jet tubes and orifices, National Heat Transfer Congress, USA, Vol.107, pp.43-50

Hussain, A.K.M.F., Zaman, M.A.Z. 1981. Turbulence suppression in free shear flows by controlled excitation. J. Fluid Mech. Vol.103, pp. 133-159

Hwang, S.D., Cho, H.H. 2003. Effects of acoustic excitation positions on heat transfer and flow in axisymmetric impinging jet: main jet excitation and shear layer excitation, Int. Journal of Heat and Fluid Flow, Vol.24, pp.199-209

Incropera, F.P., DeWitt, D.P., Bergman, T.L., Lavine, A.S. 2006. Fundamentals of heat and mass transfer, 6th edition, John Wiley and Sons Inc., USA, pp. 447-452

Jambunathan, K., Lai E., Moss, M.A and Button, B.L. 1992 A review of heat transfer data for single circular jet impingement. Int. Journal of Heat and Fluid Flow Vol.13, pp.106-115

Joint Committee For Guides in Metrology, 2008. Evaluation of measurement data - Guide to the expression of uncertainty in measurement. JCGM 100:2008

Koseoglu, M.F., Baskaya, S. 2010. The role of jet inlet geometry in impinging jet heat transfer, modeling and experiments. International Journal of Thermal Sciences Vol.49, pp 1417-1426

Kline, S.J., McClintock, F.A. 1953. Describing uncertainties in single sample experiments, Mechanical Engineering, Vol.75, pp.3-9

Maghzian, H., 2007. Simulation of hydrodynamics of the jet impingement using arbitrary lagrangian eulerian formulation, Ph.D thesis, The University of British Columbia.

Mankbadi, R.R., Raman, G., Rice, E.J., 1989, Effects of core turbulence on jet excitability, 2nd Shear Flow Control Congress, NASA Technical Memorandum, 101405, ICOMP-88-21, AIAA-89-0966

Martin, H., 1977. Heat and mass transfer between impinging gas jets and solid surfaces. J. Matter. Process. Technol., Vol.136, 1-3, pp 1-60

Martin, H., 1986. Heat exchanger design handbook. Hemisphere, pp 2.5.6-1 – 2.5.6-10

Narumanchi, S., Kelly, K., Mihalic, M., Gopalan, S., Hester R., Vlahinos, A. 2008. 24th IEEE SEMI-THERM Symposium, pp.154-162

Obot, N.Y., Mujumdar, A.S, Douglas W.J.M. 1982. Effect of semi-confinement on impingement heat transfer, Proc. 7th Int. Heat Transfer Conference, Germany, Vol.3, pp.395-400

Pavlova, A., Amitay, M. September 2006. Electronic cooling using synthetic jet impingement, Journal of Heat Transfer, Vol.128, pp.897-907

Popiel, C. O., Trass, O.1982. The effect of ordered structure of turbulence on momentum, heat, and mass transfer of impinging round jets. Proc. 7th Int. Heat Transfer Conf., Munchen, Germany, September 6-10, 6, 141-146

Popiel, C.O., Boguslawski, L. 1988. Effect of flow structure on the heat or mass transfer on a flat plate in impinging round jet, UK National Conference on Heat Transfer, Vol.1, pp.663-685

Raman,G., Zaman, K.B.M.Q. and Rice, E.J. 1989. Initial turbulence effect on jet evolution with and without tonal excitation. Phys. Fluids A 1(7).1240-1248.

Rice, E.J., Zaman, K.B.M.Q. 1987. Control of shear flows by artificial excitation, NASA Technical Memorandum 100201, AIAA-87-2722

Sagot, B., Antonini, G., Buron, F. 2010. Enhancement of jet-to-wall heat transfer using axisymmetric grooved impinging plates, Int. Journal of Thermal Sciences, Vol.49, pp.1026-1030

Sagot, B., Antonini, Christgen, A., G., Buron, F. 2008. Jet impingement heat transfer on a flat plate at a constant wall temperature, Int. Journal of Thermal Sciences, Vol.47, pp.1610-1619

Schlunder, E.U., Gnielinski, V. 1967, Heat and mass transfer between surfaces and impinging jets, Chem. Ing. Tech., Vol. 39, pp.578-584

Sibulkin, M. 1952. Heat transfer near the forward stagnation point of a body of revolution. J. Aeronautical Sci., August

Tani, I., Komatsu, Y. 1966. Impingement of a round jet on a flat surface. Proc. of the 11th International Congress of Applied Mechanics (H. Gortler, Ed.), Springer-Verlag, New York, pp.672-676

Wiltse, J. M., Glezer,A. 1992. Manipulation of free shear flows using piezoelectric actuators. J. Fluid Mech. Vol. 249, pp. 261-285

Wiltse, J. M., Glezer,A. 1998. Direct excitation of small-scale motions in free shear flows. Physics of Fluids, Vol 10, pp.2026-2036

Wolf, D. H., Incropera, F. P., Viskanta, R. 1993. Jet impingement boiling, Advances in Heat Transfer, J. P. Hartnett, T. F. Irvine, and Y. I. Cho, eds., Academic Press, Inc., Vol. 23, pp. 1–132

Zhang, J., Tan, X. 2007. Experimental study on flow and heat transfer characteristics of synthetic jet driven by piezoelectric actuator, Science in China Series E: Technological Sciences, Vol.50, pp.221-229

Zhou, D.W. and Lee, S.J. 2004. Heat transfer enhancement of impinging jets using mesh screens. Int. Journal of Heat and Mass Transfer, Vol 47, pp.2097-2108

Zuckerman, N., Lior, N. 2005. Impingement Heat Transfer: Correlations and Numerical Modeling. Journal of Heat Transfer, VOL.127, pp.544-552